

MinT: A Fast Lightweight Envelope/Monte-Carlo Beam Optics Code for the Proton Beamlines of the Paul Scherrer Institute

C. Baumgarten

*Paul Scherrer Institute, Switzerland**

(Dated: July 31, 2023)

We report about the methods used in, and the performance of, the new fast and light-weight linear beam transport program MINT. MINT provides, beyond the usual linear ion optics, methods to compute the effects of beam degradation, multiple scattering and beam collimation. This is specifically important in facilities where the ion beam passes matter, for instance in proton therapy beamlines with an energy degrader as in the Proscan facility at PSI, but also for modeling the beam traversing the Muon- and Pion-production targets of the Paul Scherrer Institut's high intensity proton accelerator (HIPA). MINT is intended to be useful as a support tool for the HIPA and Proscan control rooms. This requires to have useful results within a few seconds. Hence simplicity and speed of calculation is favored against higher accuracy.

MINT has been designed not only to replace the FORTRAN 77 codes TRANSPORT and TURTLE, but to combine and extent their capabilities. MINT is a byte-code-compiler which translates an input language, described by syntactic rules. This allows for control structures like "if-then-else" or "while"-loops, thus providing a high flexibility and readability.

arXiv:2202.07245v2 [physics.acc-ph] 28 Jul 2023

* christian.baumgarten@psi.ch

I. INTRODUCTION

The Paul Scherrer Institute (PSI) in Villigen, Switzerland, is known for its high intensity proton accelerator (HIPA) [1–3] which held for many years the world record of proton beam power (up to 1.4 MW). PSI is also known for pioneering research of proton tumor therapy in the center for proton therapy (CPT) and its facility Proscan [4].

Both facilities are driven by cyclotrons and in both facilities the simulation of the proton beam optics faces the problem to describe beams of several ten to some hundred MeV passing through matter with subsequent beam collimation: In the HIPA facility, the 590 MeV proton beam has to pass through two graphite wheel targets before it is sent to the SINQ spallation neutron source. In case of Proscan, the beam passes through an adjustable graphite wedge degrader to tune the beam energy and hence the range of the protons in the target tissue.

The HIPA facility, shown in Fig. 1 is driven by an accelerator chain consisting of a Cockcroft-Walton-type pre-accelerator and two isochronous separate sector cyclotrons, namely the 72 MeV Injector II and the Ring cyclotron, providing a 590 MeV proton beam of up to 2.4 mA. This high intensity beam is either sent to the ultra-cold neutron source “UCN” [5–11] or via two graphite targets, the 5 mm thick *Target M* and the 40–60 mm thick *Target E* [12–14], to the Swiss spallation neutron source “SINQ” [15–20].

The Proscan therapy (PT) facility is driven by a 250 MeV superconducting compact cyclotron “COMET” with currents of (usually) up to $1\ \mu\text{A}$ [21–29]. After extraction from COMET, the 250 MeV beam passes a double-wedge degrader which is used to reduce the beam energy to 74–230 MeV. The energy degradation increases the emittance

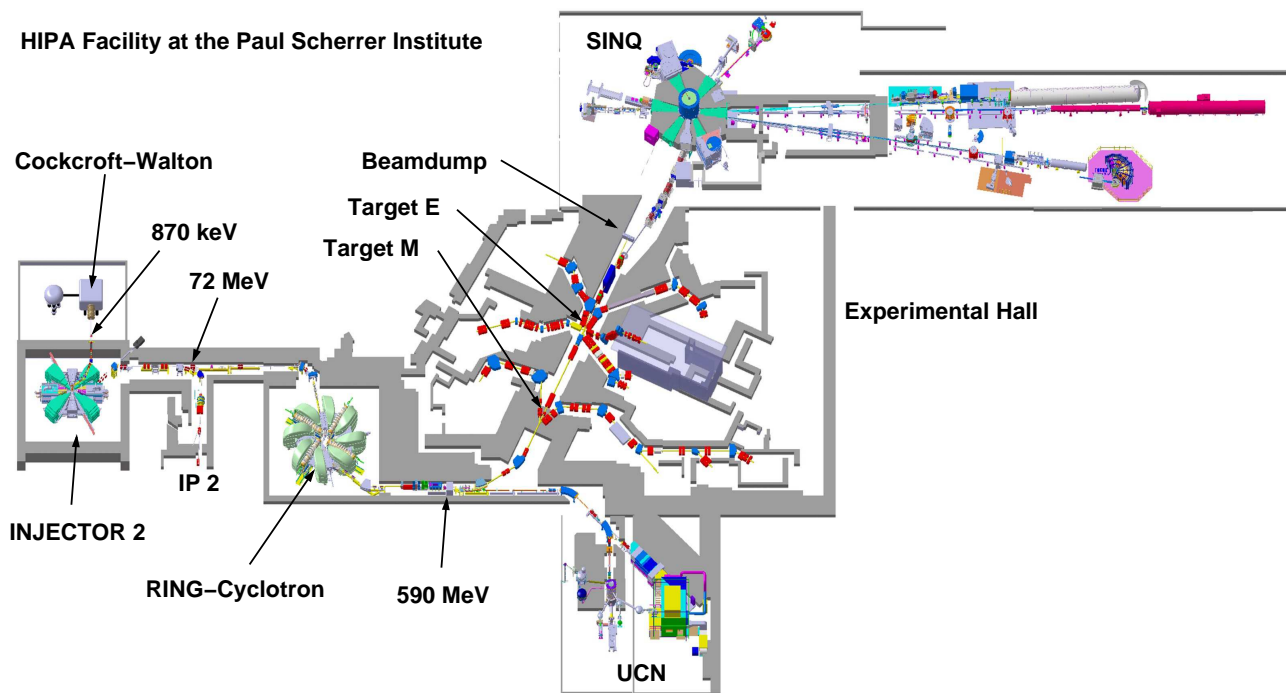


FIG. 1. Overview over HIPA facility at PSI. Here we are concerned specifically with the beamlines, the 870 keV injection beamline “BW870”, the 72 MeV-beamline “IW2”, connecting Injector 2 with the Ring cyclotron and the 590 MeV beamline, the so-called “p-Channel”, which guides the proton beam from the Ring cyclotron via Target M and Target E to beamdump and SINQ, respectively.

and energy spread by multiple Coulomb scattering. After energy degradation, the beam has to be collimated and the energy spread reduced in order to match the acceptance of the beam transport system. Furthermore, the degraded beam passes several thin monitors and vacuum windows before entering a treatment room.

In any accelerator facilities it is highly desired to have a fast beam-optics software to support control room work, like the prediction of beam envelopes, the fit of envelopes to measured profiles or the development of new tunes. A Beam dynamics code that is supposed to be useful for both, the HIPA and Proscan beamlines, must hence be able to model the effects that degraders and collimators have on beam parameters like energy, emittance and beam divergence. Up until recently, the only online beam dynamics code used in the HIPA control room was Urs Rohrer’s graphical version of TRANSPORT [30–32]. The Proscan control rooms had no beam dynamics tool at all, since the use of TRANSPORT and TURTLE [33, 34], though possible in principle, turned out to be too cumbersome to support daily work in the control rooms. High-accuracy codes like OPAL[35–39], GEANT [40–42], or the Geant-based BDSIM [43], do exist, but are better suited for high-accuracy offline studies, preferably executed on high performance computers.

MINT¹ is a lightweight beam optics code designed to support control room activities, for instance for beam tuning and development, that allows to provide reasonably accurate answers in short times (a few seconds up to a minute) instead of highly accurate results within tens of minutes or hours. Though MINT has been specifically designed as an online tool, it is useful offline as well, as a design-tool for the layout of new beam lines, when the speed of calculation and the flexibility of the code are essential as well. Since modern control room computers are mostly using Linux as operating system, MINT is a Linux-program as well. Other operating systems are not (yet) supported. However, MINT is fast enough for the use in virtual machines.

In the following we report about the features and performance of MINT, the methods used in the program and demonstrate it’s capabilities to model the beam optics of the beamlines which are part of PSI’s proton facilities.

II. THE BEAM OPTICS PROGRAM MINT

A precursor of MINT was developed for the Gantry 3 project at PSI [45–49]. The main idea was to model the transition through matter (i.e. energy degrader) by fast and simple approximations and through collimators by a “removal on hit” strategy with a Monte-Carlo-ensemble created from the matrix of second moments. This is a pragmatic “engineering” kind of approach which often is sufficient in accuracy with respect to the transmitted beam. MINT is a complete re-write of this first code, which is now controlled by a programming style input file with capabilities for graphical output to screen and to all file formats supported by the GNU plotutils library (notably Postscript, PNG and FIG).

A. Optics Calculations in MinT

The ion optics machinery of MINT is based on the linear beam optics methods known from the programs TRANSPORT and TURTLE, i.e. the beam is described by it’s first and second moments in local co-moving coordinates. If

¹ (M)int (i)s (n)ot (T)ransport [44].

$X = (x, x', y, y', z, \delta)^T$ are the usual six phase space coordinates in the co-moving frame ², then the first moments are $X_i(s) = \langle X_i \rangle_s$ and second moments are given by a symmetric matrix $\Sigma_{ij}(s) = \langle (X_i - \langle X_i \rangle) (X_j - \langle X_j \rangle) \rangle_s$. The particle transport through beam optical elements, using a linear ³ approximation and hard-edge magnets, is then given by a sequence of multiplications with symplectic matrices \mathbf{M}_k . MINT allows to control the stepsize in all beamline elements individually and can therefore be optimized by the user either for speed or for accuracy. It is possible, but not always desired, to compute the transfer matrix of some element in one step, since beam-loss typically occurs inside of quads and bends. Possible beam-loss in the center of magnets can only be estimated with reasonable accuracy, if the beam optics inside the element is calculated in small steps. MINT evaluates beam losses only when the envelope is evaluated as well (i.e. *after* some step). MINT possesses two modes, a pure envelope mode, corresponding to linear TRANSPORT calculations, and a Monte-Carlo assisted envelope mode (“sampled mode”), where the beam is represented by a Monte-Carlo generated ensemble of “rays” X_i . The user can switch between these modes by the insertion of dedicated elements.

In envelope mode the equations are:

$$\begin{aligned} X(s+L) &= \mathbf{M}_k(L) X(s) \\ \Sigma(s+L) &= \mathbf{M}_k(L) \Sigma(s) \mathbf{M}_k(L)^T \end{aligned} \quad (1)$$

where s is the position along the reference trajectory, L is the length of the calculation step in element k and \mathbf{M}_k is the transfer matrix of the k -th element. MINT is equipped with an integrated symplectic Monte Carlo generator for multivariate Gaussian distributions [50]. A distribution of n trajectories is represented by a $6 \times n$ -matrix \mathbf{X}_{ij} , such that the center of the bunch is given by

$$X_i(s) = \frac{1}{n} \sum_{j=1}^n \mathbf{X}_{ij}(s) \quad (2)$$

and the centered distribution $\tilde{\mathbf{X}}_{ij}$ by

$$\tilde{\mathbf{X}}_{ij} = \mathbf{X}_{ij}(s) - X_i(s). \quad (3)$$

The matrix of second moments is then

$$\Sigma_{ij} = \frac{1}{n} \tilde{\mathbf{X}} \tilde{\mathbf{X}}^T \quad (4)$$

Without collimators, the evolution of the beam centroid, MC-sample and matrix of second moments is described by a symplectic transfer matrix $\mathbf{M}(L)$ and is in Monte-Carlo mode given by:

$$\begin{aligned} \mathbf{X}(s+L) &= \mathbf{M}_k(L) \mathbf{X}(s) \\ \Sigma(s+L) &= \tilde{\mathbf{X}}(s+L) \tilde{\mathbf{X}}(s+L)^T \end{aligned} \quad (5)$$

In Monte-Carlo-mode, the Σ -matrix is obtained from the (possibly re-centered) Monte-Carlo-sample.

In the presence of collimators, the MC-sample is “filtered”: trajectories which hit a collimator, are removed from the ensemble \mathbf{X} which represents the beam. The current version of MINT allows for circular, elliptic and rectangular

² Where the dash indicates the derivative along the beam path $x' \equiv \frac{dx}{ds}$ and $\delta = \frac{dp}{p}$ is the momentum spread.

³ MINT, starting with version 0.50, supports second order calculation. But since second order effects are weak in the PSI proton beamlines, only first order has been compared and tested against measurements.

collimators and moveable horizontal or vertical, symmetric or asymmetric, slits. If $X = (x, x', y, y', z, \delta = \frac{dp}{p})^T$ is the vector of local coordinates, then a trajectory passes an elliptic collimator with horizontal and vertical half-diameter a and b , if

$$\frac{(x + x_0)^2}{a} + \frac{(y + y_0)^2}{b} \leq 1 \quad (6)$$

where x_0 and y_0 are the coordinates of the beam centroid.

No scattering calculations are done on collimators. But in many beam optical calculations, it is not the primary objective to obtain a detailed calculation of losses and activation, but the knowledge of the properties of the fraction of the beam which passes the collimator. The test Eq. 6 of $10^4 - 10^6$ trajectories is computationally expensive, but the simplest general scalable method to solve the (strongly non-linear) collimation problem.

B. Beam Degradation

Besides collimation, the main task appearing for instance in proton therapy beamlines with beam degrader is the calculation of beam degradation effects, such as energy reduction and -straggling, and emittance increase by multiple scattering [51–55].

1. Energy Degradation

For the energy loss (and range) calculations the Bethe-Bloch-formula is used to describe the average energy loss per unit length of charged particles passing through matter [56]:

$$\frac{dE}{ds} = -K z^2 \frac{Z}{A} \frac{1}{\beta^2} \left[\frac{1}{2} \log \left(\frac{2 m_e c^2 \beta^2 \gamma^2 T_{max}}{I^2} \right) - \beta^2 - \frac{\delta}{2} \right]. \quad (7)$$

where s is the pathlength, m_e is the electron mass, z and M are the charge number and the mass of the projectile, N_A is Avogadro's constant, Z and A are atomic number and mass of the medium (in $g mol^{-1}$), and K is the factor $K = 4 \pi N_A r_e^2 m_e c^2$. Furthermore r_e is the classical electron radius $r_e = \frac{e^2}{4 \pi \epsilon_0 c^2}$, $\beta = \frac{v}{c}$ is the velocity in units of the speed of light c , and γ is the known relativistic factor $\gamma = \frac{1}{\sqrt{1-\beta^2}}$. I is the mean excitation energy in units of eV , δ is the density effect correction to ionization energy loss, and T_{max} is finally given by

$$T_{max} = \frac{2 m_e c^2 \beta^2 \gamma^2}{1 + 2 \gamma m_e / M + (m_e / M)^2}. \quad (8)$$

The current version of MINT neglects the *density effect correction term* (i.e. $\delta \rightarrow 0$) as the contribution is negligible in the energy range below about a GeV [56].

In case of degraders made from composite materials (containing different nuclei), MINT computes the energy losses for each target component with the corresponding reduced density:

$$\frac{dE}{ds} = -\frac{K z^2}{\beta^2} \sum_k \frac{Z_k}{A_k} \rho_k \left[\log \left(\frac{2 m_e c^2 \beta^2 \gamma^2}{I_k} \right) - \beta^2 \right], \quad (9)$$

where the *partial* densities ρ_k have to sum up to the density of the compound ρ :

$$\rho = \sum_k \rho_k. \quad (10)$$

For the convenience of use, MINT provides the possibility define arbitrary pure and composite materials.

2. Energy Straggling

The conventional 6th beam coordinate $\delta = \frac{\delta p}{p_0}$ is a relative quantity and with the degradation process, both the momentum spread δp and the average momentum p_0 , change. The former increases by energy straggling while the latter decreases by energy degradation.

The latter means that the final energy E_f depends, after the passage through a slab of fixed thickness Δs , nonlinearly on the initial energy E_i , so that

$$\frac{dE_f}{dE_i} = \frac{dE_f/ds}{dE_i/ds} \quad (11)$$

and hence

$$\sigma_{E_f}^2 = \left(\frac{dE_f/ds}{dE_i/ds} \right)^2 \sigma_{E_i}^2. \quad (12)$$

The combination with the stochastic straggling yields [57]:

$$\sigma_{E_f}^2 = \left(\frac{M(E_f)}{M(E_i)} \right)^2 \left(\sigma_{E_i}^2 + M(E_i)^2 \int_{E_f}^{E_i} \frac{N(T)}{M(T)^3} dT \right), \quad (13)$$

where $M(E) = -\frac{dE}{ds}$ and $N(E)$ is the stochastic energy straggling for thin targets (in dependence on energy), which can be calculated by [58]:

$$\begin{aligned} N(E) &= \frac{d\sigma_E^2}{ds} = 4\pi N_a r_e^2 (m_e c^2)^2 \rho \frac{Z}{A} \left(1 - \frac{1}{2}\beta^2\right) \gamma^2 \\ &= 4\pi N_a r_e^2 (m_e c^2)^2 \rho \frac{Z}{A} \frac{1 + \gamma^2}{2} \end{aligned} \quad (14)$$

where ρ is the density, Z the nuclear charge and A the mass number of the scatterer. If we change the integration variable in Eqn. 13, we obtain in the limiting case $\Delta x \rightarrow 0$:

$$\begin{aligned} \frac{\sigma_{E_f}^2}{M(E_f)^2} &= \frac{\sigma_{E_i}^2}{M(E_i)^2} + \int_0^{\Delta x} \frac{N(E(x))}{M(E(x))^2} dx \\ \frac{d}{ds} \left(\frac{\sigma_E^2}{M(E)^2} \right) &= \frac{N(E)}{M(E)^2} \end{aligned} \quad (15)$$

It is hence necessary to normalize the energy variance with the (absolute value of) the Bethe-Bloch function $M(E)$ in order to obtain, in Gaussian approximation, the desired differential equation. Eq. 15 can be integrated numerically to finally obtain σ_E^2 at the final energy E_f and hence the final momentum spread δ .

3. Deep Inelastic Scattering

MINT enables to estimate the beam loss by deep inelastic scattering (DIS) by the formula provided in Ref. [59–61] for energies between a few MeV and a few hundred MeV. Any projectile that is subject to some inelastic process, is counted as lost. But MINT does not remove tracks due to DIS, but simply calculates the surviving fraction of the beam. The beam current is then reduced along the beam path accordingly.

The DIS calculation requires that the user specifies the RMS radius R_{rms} for the projectile and passed material. Then an inverse scattering length $\frac{1}{\lambda_{DIS}}$ can be written as

$$\frac{1}{\lambda_{DIS}} = \frac{\rho}{A} \sigma_{DIS} \quad (16)$$

The beam current change dI for passing a slab of thickness dx is then approximated by

$$\frac{dI}{ds} = -\frac{I}{\lambda_{DIS}} \quad (17)$$

Hence the surviving fraction of particles without deep inelastic process decreases exponentially with the thickness of the traversed matter.

4. Emittance Increase by Lateral Straggling

MINT provides two scattering models, the first follows the suggestion of Francis Farley [62, 63], which is a “local” approximation of the Moliere theory. Farley refers to Ref. ([56]) where the precision is claimed to be 11%. The theoretical description of the beam passage through the solid degrader material can best be understood, if one considers an idealized parallel beam (zero emittance) interacting with a single scatterer. The immediate effect of the scatterer is to change *only angle* (and energy) of the incident proton (or ion). The time derivative of the matrix σ of second moments is then given (in one dimension) by [63]:

$$\frac{d\sigma}{ds} = \begin{pmatrix} 2\sigma_{12} & \sigma_{22} \\ \sigma_{22} & T(p) \end{pmatrix}, \quad (18)$$

where $T(p)$ is the scattering power. Farley used $T_{FF}(p) = \frac{K}{p^2\beta^2}$ as scattering power where $p = p(s)$ is the momentum, $\beta = \beta(s) = v(s)/c$ is the ratio of the projectile’s velocity to the velocity of light and K is a material dependent constant that is given by Farley as:

$$K = 200 (\text{MeV}/c)^2 \frac{Z^2}{X_0}, \quad (19)$$

with the charge of the projectile Z and the radiation length of the target material X_0 [56] given in units of $[\text{g cm}^{-2}]$:

$$X_0 = \frac{716.4 A}{Z(Z+1) \log(287/\sqrt{Z})}. \quad (20)$$

Often an alternative radiation length $\tilde{X}_0 = X_0/\rho$ is used, which is divided by the target density ρ and then has the unit [cm].

According to Gottschalk, this corresponds to the scattering power of Fermi and Rossi [64]:

$$T_{FR} = \left(\frac{E_s Z}{p \beta} \right)^2 \frac{1}{X_0}, \quad (21)$$

where $E_s = 15 \text{ MeV}$ approximately matches Farley’s formula. Gottschalk presented a detailed comparison of various theoretical models in Ref. ([64]) and derived a phenomenological model to match the experimental data. His scattering power is

$$T_{GS} = f_{dM} \left(\frac{E_s Z}{p \beta} \right)^2 \frac{1}{X_S}, \quad (22)$$

the end of the element, the matrices of both ensembles are added, which means that the direction of each trajectory is changed statistically.

III. EXAMPLES: MINT FOR PSI BEAMLINES

In this section we provide some example applications of MINT, namely to the PSI proton beamlines.

A. HIPA Beamlines

Fig. 1 gives an overview of the HIPA facilities [3]. The beam is generated in a compact ECR proton source [65] and extracted with a 60 kV extraction system which is located on the high voltage platform of the 810 kV Cockcroft-Walton accelerator. The resulting 870 keV DC beam with a current of 10 – 12 mA is send through a system of two bunchers, a 50 MHz first and a 150 MHz third-harmonic buncher, to the axial injection line of Injector II. Injector II is a 72 MeV high-current isochronous cyclotron with four separate sectors [66–71]. After extraction, the beam is send via the 72 MeV-beamline “IW2” to the so-called “Ring-cyclotron” [72–78] where it is accelerated to 590 MeV. A fraction of several ten μA can be split off from the 72 MeV-beam and send to the isotope production facility IP2. The 590 MeV beam is either transported to the ultra-cold neutrons at UCN (typically in “pulses” of a few seconds) or otherwise send to the muon/pion production graphite targets, first the 5 mm thick “Target M” and then to the 40 – 60 mm long “Target E”. After an appropriate collimation, the remaining useable beam is either send to the SING-target for neutron production or otherwise to a high-intensity beam dump ($I_{max} \approx 1.7 \text{ mA}$).

Since TRANSPORT offers no convenient possibility to simulate the passage of high-energy particles through matter, the description of this beamline with TRANSPORT requires to split the optics calculation from Ring-cyclotron to SING (or beamdump) into at least 3 sections, from Ring to *Target M*, from *Target M* to *Target E* and from *Target E* to beamdump or SING, respectively. Each of this sections is then treated seperately and it is up to the user to verify the overall consistency. The MINT monte-carlo-mode (activated here behind *Target M*) allows not only to compute the beam optics in one go, but also to predict beam currents and “realistic” (non-Gaussian) beam profiles. In the following we provide some examples.

1. From Ring Cyclotron to the Beamdump

Fig. 2 shows the result of a MINT optical calculation from Ring cyclotron to the beamdump for two versions of *Target E*, 60 mm and 40 mm long (at $s \approx 61 \text{ m}$). The symbols are measurements of the latter. The apertures of the respective beamline components are indicated by a colored background in PSI convention, i.e. blue for bends, red for quads, gray for drifts and yellow for steering magnets. The graphical output follows the TRANSPORT conventions, i.e. the vertical beam size ($2\sigma_{rms}$) is shown above axis (red) and the horizontal beam size (blue) below axis. The symbols indicate the beam size as measured by beam profile monitors.

The primary beam intensity was (60 mm target) 1840 μA , the beam intensity after collimation (measured by current monitor MHC5) was 1022 μA , the MINT prediction is 1090 μA using Gottschalk’s scattering power (1054 μA for the

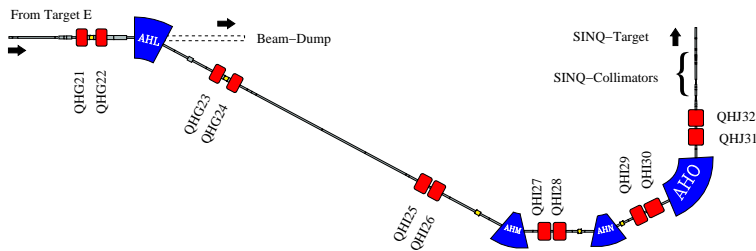


FIG. 3. Beamline from switching-magnet AHL towards the spallation neutron source SINQ, shown as a side-view: the beam enters the SINQ target from below.

modified version). In case of the 40 mm target, the measured (simulated) current after *Target E* was $1120 \mu\text{A}$ ($1111 \mu\text{A}$), using the modified version of Gottschalk’s scattering power.

These calculations used a Monte-Carlo sample of 50000 “macro”-particles (Monte-Carlo mode starting behind *Target E*) and took less than five seconds on an average laptop computer ⁴. The prediction of the correct beam current depends on many details so that the agreement with the measured currents is quite satisfactory.

After the passage of *Target M*, the estimated beam energy is calculated to be 586.6 MeV, after the 40 mm (60 mm) long *Target E* it is 569.3 MeV (560.6 MeV). The emittance values assumed at the exit of the Ring cyclotron are $\varepsilon_x = 0.154$ mmmrad and $\varepsilon_y = 0.366$ mmmrad, after *Target M* they increase to $\varepsilon_x = 0.468$ mmmrad and $\varepsilon_y = 1.63$ mmmrad, after *Target E* (40 mm) to $\varepsilon_x = 1.035$ mmmrad and $\varepsilon_y = 5$ mmmrad. The MINT simulation results in a beam loss of 1.1 % in *Target M* and of 8.24 % in *Target E*, which agrees well with the numbers given in Ref. [79] ⁵.

2. From Ring Cyclotron to SINQ

Since the installation of the SINQ, the beamdump is used only in times when the SINQ is not ready for data taking. In SINQ operation, the magnet AHL is active and the SINQ-beamline guides the beam downwards in order to inject it from below into the SINQ target (see Fig. 3) [82]. The SINQ-beamline is equipped with some large aperture quadrupoles. Rohrer’s version of TRANSPORT supports large aperture quads by a fringe field corrections derived from fringe field integrals [30] according to the approximation developed by Matsuda and Wollnik [83]. However, the suggested corrections are not symplectic. Furthermore the calculation of the fringe field integrals requires a precise knowledge of the field shape, which is not always available and/or reliable. Nonetheless MINT provides a symplectified version of this method, described in Sec. B. Furthermore MINT allows to choose another (fully symplectic) correction due to Baartman which does not require the knowledge of the fringe field integrals. In case of the SINQ beamline it provides an equivalently satisfying agreement with the measured beam profiles.

If f is the (uncorrected) focusing length of the quad R the pole radius and L the effective length, then the Baartman’s correction is based of the following change of the focusing length [84]:

$$\Delta f = R^2/(2L) \quad (25)$$

A more detailed description of the implementation in MINT is given in Sec. B of the appendix.

Both methods are able to describe the optics of the SINQ beamline with satisfactory accuracy. Fig. 4 shows the results using a MC sample of 10^4 particles with Baartman’s fringe field correction. The profile measurements between

⁴ The speed of calculation can vary significantly, depending on the used step size. The calculations shown here included a space-charge kicks at least every 100 mm.

⁵ More details on the collimators can be found in Refs. [79–82].

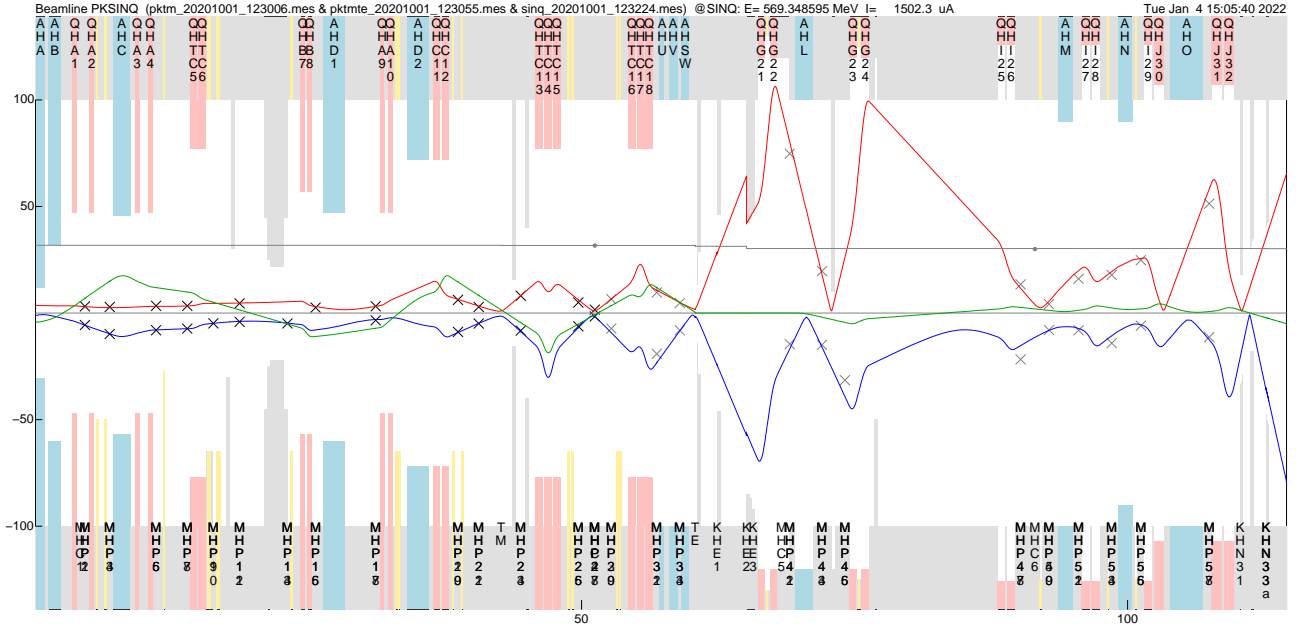


FIG. 4. Beam envelope from Ring cyclotron to SINQ target with the 40 mm long *Target E* (Data from 2021 Production). The measured current towards SINQ was $955 \mu\text{A}$, the prediction of MINT is $952 \mu\text{A}$ with the modified version of Gottschalk’s scattering power. The (scaled) dispersion is shown as a green solid line. The apertures of magnets and collimator are indicated by the respective background colors. The gray line (symbols) represent the calculated (measured) beam current.

Ring (start) and Target M (labeled “TM”) were used to match the starting conditions. The remaining beamline (Target M up to SINQ) is a forward calculation. The execution time on an average laptop (including fit) was about 6 s.

Even though the predicted losses can deviate from the measurements by a few percent, MINT allows for a reasonable online prediction of the beam optics. In a high current facility like HIPA, where even small losses, in the order of a permille, can overheat and melt components, the accuracy of the MINT model is certainly not sufficient to omit the fine tuning by operators. However approximate beam tunes can be elaborated and fine-tuned by a stepwise increase of the beam current to its production value.

However, for (the commissioning or tuning of) low intensity beamlines like the ones used for proton therapy machine, MinT provides sufficient numerical accuracy to compute tunes which require little or no correction by manual fine-tuning.

3. Injector II and the 72 MeV-beamline

The 72 MeV beamline (“IW2”) connects the extraction of injector II with the injection of the Ring cyclotrons [85]. As reported elsewhere [86–92], the Injector II cyclotron is operated in the space-charge dominated regime. MINT provides the possibility to define a sequence of elements as a “ring” so that the matched beam matrix Σ_m can be derived from the matching condition, for given emittances and current. The specific problem in case of non-negligible space charge is the fact that the one-turn-transfer matrix depends on the strength of the space charge and hence on

the beam size. If $\mathbf{M} = \mathbf{M}(I, \varepsilon_i)$ is the one-turn-transfer-matrix, depending on beam current I and beam emittances ε_i , then the beam is matched, iff

$$\mathbf{S} = \mathbf{M} \mathbf{S} \mathbf{M}^{-1}, \quad (26)$$

where - with \mathbf{J} as the symplectic unit matrix - the matrix of second moments for the matched distribution is given as $\Sigma_m = \mathbf{S} \mathbf{J}$. MINT makes use of the general decoupling/diagonalization methods described in Refs. [50, 93–95], which allow to determine \mathbf{S} and hence Σ for arbitrary symplectic transport matrix \mathbf{M} and given proper eigen-emittances. However, here \mathbf{M} depends itself on (elements of) the Σ -matrix, for instance on (square of the rms) beam size, then the problem can not be solved analytically and it is required to use an iterative scheme [89]. MINT is equipped with such a scheme and, for the beam conditions and currents of Injector 2, typically less than 10 iterations are required to find the matched beam. With low beam current or if space charge is ignored, ideal isochronous cyclotrons do not provide any longitudinal focusing and the matching is hence undefined in the longitudinal direction.

The matched beam is then used as a starting condition for a fit to the measured profiles of the 72 MeV beamline which connects Injector II and the Ring cyclotron. The MINT calculations confirmed that the matched beam assumption provides excellent starting conditions which allow to fit the beam envelope of the IW2-beamline in few steps. At high currents, the horizontal beam envelope requires almost no adjustments to match the measured beam sizes.

In linear approximation, the cyclotron specific space charge effect connect only horizontal and longitudinal motion, while the vertical motion is not affected. In other words, within Injector II, the vertical beam size is not directly coupled to the horizontal and longitudinal motion and hence can be fitted to the measured beam sizes without strong influence on the so-called “vortex motion” [89, 90, 92].

Fig. 5 shows the two stages of the fitting procedure. The darker colors show the beam envelopes of a two-parameter fit (varying only two beam emittance values), assuming a matched beam from Injector II. In the second step, the vertical initial beam parameters (σ_{33} , σ_{34} , σ_{44}) are varied to improve the fit to the vertical beam sizes. On the left the simulation starts with the last turn of Injector II (four bends) and ends on the right with the first turn of the Ring cyclotron (eight bends). For a comparison with OPAL see Ref. [85].

The results confirm that the horizontal and longitudinal beam parameters are due to the space-charge induced coupling, while the vertical beam parameters are linearly independent. This kind of horizontal-longitudinal “self-matching” works, as expected, only for sufficiently high beam currents. There is no passage through matter and no significant beam collimation in the 72 MeV transfer line and MINT is therefore operated here in pure envelope mode.

4. The 870 keV-beamline

Fig. 6 gives a schematic overview of the 870 keV “BW870” injection line connecting the ECR ion source via Cockcroft-Walton DC preaccelerator with the center of Injector 2 [67, 70, 96–98]. Due to the strong space charge forces of the 10 mA DC beam, the beamline BW870 is most challenging in terms of ion-optical modelling. The specific difficulty is due to (partial) space charge compensation by electrons which are attracted and captured by the DC proton beam potential. Furthermore, the DC proton beam is bunched by a first and third harmonic buncher [71, 99]. The main task is here is to find a method to model the transition from a DC beam into a bunched beam. The bunching process involves all possible phases of the buncher and can therefore not be modelled in linear approximation.

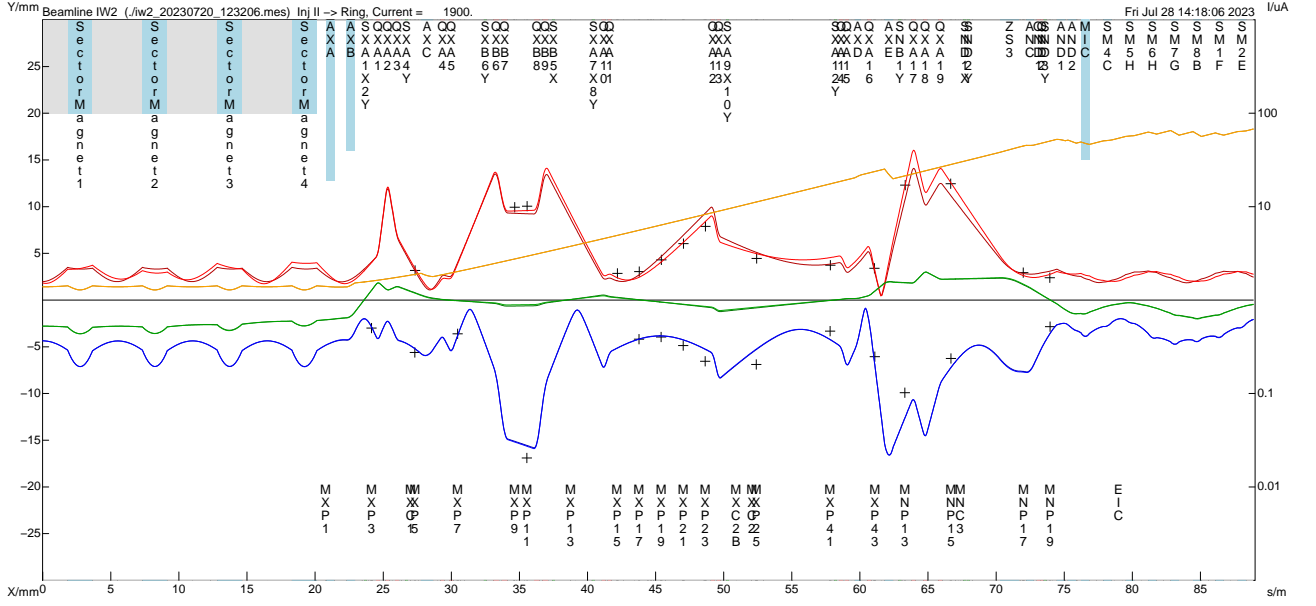


FIG. 5. Beam envelopes (2σ) from the last turn of Injector II to the first turn of the PSI Ring cyclotron. For the fit, it is assumed that the transverse horizontal equals the longitudinal emittance ($\varepsilon_{x,z} = \varepsilon_x = \varepsilon_z$). The emittances $\varepsilon_{x,z}$ and ε_y are fitted to the measured beam profiles, under the assumption that the beam is matched to the last turn of Injector II [89, 94]. The vertical (horizontal) envelopes are shown in dark red (blue). The “+” symbols indicate the respective beam sizes as measured by profile monitors and the light colored (red/blue) lines indicate the results of MINT envelope calculation before and after a fit of the axial beam parameters to fit the measured beam sizes. The corresponding initial (final) dispersion is shown in dark (light) green and the longitudinal beam dimension (scaled down by four) in (dark/light) orange. The computation, including all fits, takes a few seconds on an average personal computer. In case of the IW2 beamline, where space charge has to be included, the computation speed depends strongly on the settings. In the plot shown here, the distance between two subsequent space charge kicks was 50 mm.

A rather simple method to model the effect of a buncher in combination with a DC beam has been implemented in MINT. This method presumes a sampled beam. Since the beam of the 870 keV beamline has passed a Cockcroft-Walton type DC accelerator, the energy spread of the beam entering the buncher is very low and the bunch-length is undefined.

The buncher element therefore has to introduce and (re-) define the bunch length using the buncher-frequency f_b and the particle velocity v . Hence a MINT-buncher re-samples the longitudinal distribution assuming a bunch length σ_z which is an appropriate fraction of v/f_b . In case of the 870 keV-beamline, one obtains

$$v/f_b = 255 \text{ mm} \quad (27)$$

MINT uses typically 2σ -values, and hence the bunch length is assumed to be approximately 4σ in total, so that

$$\sigma_z \approx \frac{1}{4} v/f_b. \quad (28)$$

After generating a random longitudinal position with this σ_z , the energy (i.e. momentum deviation) of each particle is adjusted accordingly, i.e. the energy change ΔE_i of the i -th particle is modified by

$$\Delta E_i = -Q V_b \sin(2\pi z_i/\sigma_z). \quad (29)$$

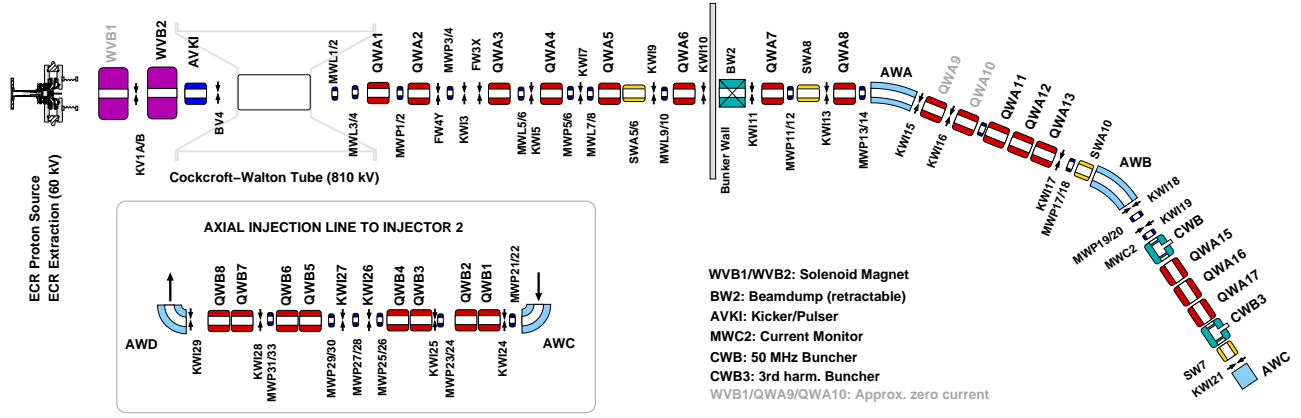


FIG. 6. Schematic overview of the HIPA beamline BW870 from ECR Ion source to Injector 2.

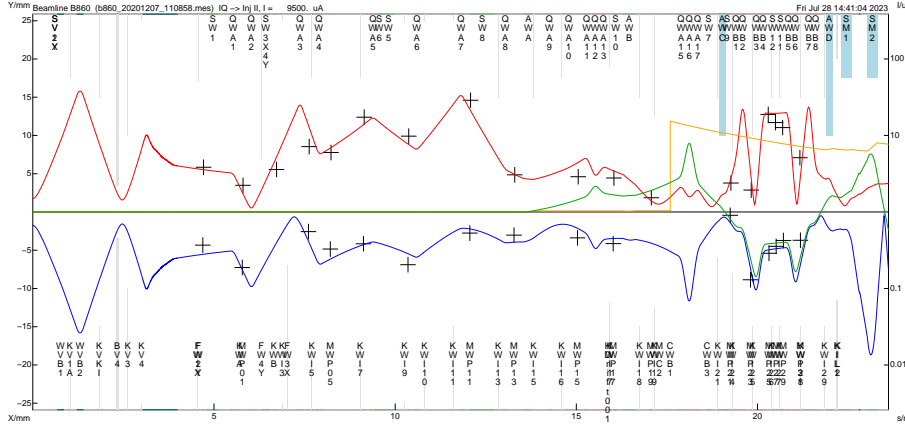


FIG. 7. Beam envelopes of the BW870 beamline. The bunch length σ_{55} is shown in orange, but scaled down (here) by a factor 10. It is undefined (zero) up to the first harmonic buncher CWB.

where V_b is the buncher voltage. The (linear) evolution of the longitudinal phase space between buncher and injector is shown in Fig. 8. The core of the formed bunches becomes longitudinally compact, and has a momentum spread of $\sigma_\delta = 0.00682$.

Fig. 9 provides a qualitative and quantitative comparison of the beam profiles in the axial injection line. Since the dispersion at the location of the profile monitors is non-zero, the (strongly non-Gaussian) energy distribution induced by the two bunchers becomes visible in the beam profiles.

There have been simulations of the bunching process of a DC beamline with space-charge presented in the past [99]. The advantage of the method implemented in MINT is that it allows to compare the simulation results with beam profile measurements, and hence to validate the used model.

B. The Proton Therapy Beamlines

Fig. 10 provides an overview of the Proscan facility [100, 101], where proton beams in an energy range between 70 and 230 MeV are used to irradiate tumors for cancer therapy, taking advantage of the so-called bragg peak [51–53, 55].

The compact isochronous cyclotron “COMET” provides a continuous wave (CW) beam of 250 MeV with currents of up to 800 nA [21–28]. The beam energy is adjusted by means of a double-wedge-degrader made from high-density graphite, followed by a beam collimation system and the energy selection system (ESS). The collimation system consists of two multi-aperture collimators KMA3 and KMA5 and some fixed collimators (KMA4, KMA6 and

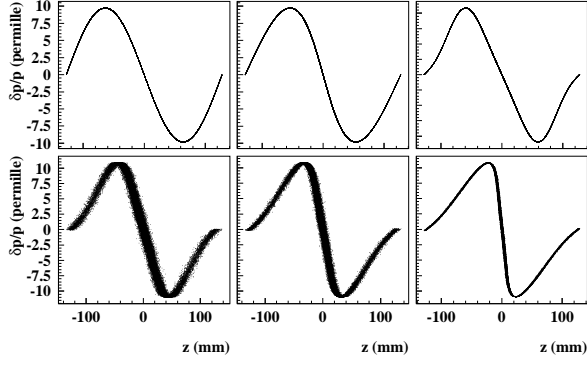


FIG. 8. Evolution of the longitudinal phase space of the 870 keV injection beamline between from buncher (upper left) up to the first turn of Injector 2 (lower right). The individual locations are (left to right), 50 MHz-buncher, before and after 3rd harmonic buncher, two positions in the vertical injection line (before QWB4 and after QWB6) and finally in the first turn of Injector 2. The 50 MHz-buncher is assumed to have a total voltage (both gaps summed up) of 17.1 kV, the 3rd harmonic buncher of -2.25 kV.

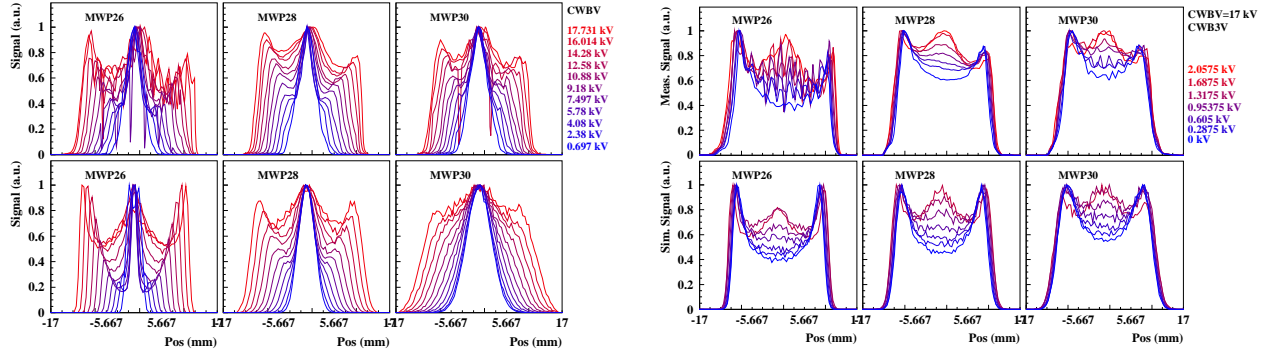


FIG. 9. Beam profiles of MWP26, MWP28 and MWP30 in the dispersive section of the axial injection line after the bunchers, for various voltages of buncher CWB with constant voltage (2.57 kV) of the third harmonic buncher CWB3 (left). Right: CWB at 17 kV with various voltages of CWB3. The measured (simulated) profiles are shown in the top (bottom) row. The profiles are centered and normalized to the same maximal value for better comparison.

KMA7) [102]. A fast kicker magnet and beam blocker BMA1 in front of the degrader are used to quickly switch the beam on or off.

The Proscan facility uses beams in the range from 70 MeV to about 230 MeV for patient treatment, controlled by the degrader wedge positions, but never the direct cyclotron beam. The transversal beam emittance therefore depends on the collimator geometry – even at the highest clinical energy of 230 MeV – but only weakly on the cyclotron beam emittance – as long as the beam is well-focused onto the center of the degrader wedges.

The (multivariate) Gaussian Monte-Carlo generator implemented in MINT approximates the beam distribution from the matrix of second moments by:

$$f(z) = \frac{f_{DIS}}{(2\pi)^2 \sqrt{|\Sigma_t|}} \exp(-z^T \Sigma_t^{-1} z/2), \quad (30)$$

Here only the transversal coordinates are of interest and therefore $z = (x, x', y, y')$ are the transversal coordinates and Σ_t is the transversal matrix of 2nd moments. But since the collimators KMA3 and KMA5 select the beam in the vicinity of the forward direction, the transmitted intensity I passing the collimators on axis (or better: close to the

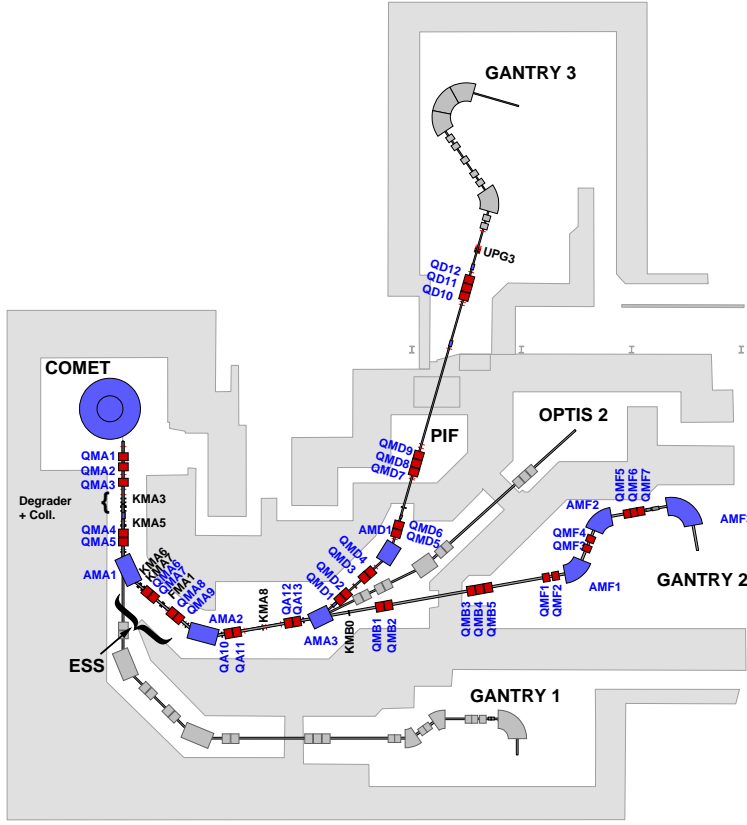


FIG. 10. Layout of the Proscan facility at PSI with the 250 MeV superconducting cyclotron “COMET”, Degradator/Collimator (KMA3 and KMA5), energy selection system ESS, Gantry 1 [103] (now in the decommissioning-phase), Gantry 2 [104], the eye treatment facility OPTIS 2 and the new Gantry 3. The proton irradiation facility (PIF) [105] is located in the Gantry 3 beam path. Dipole magnets are drawn as blue, quadrupoles as red boxes. KMA8 and KMB0 are collimators used for intensity compensation.

axis) can be approximated by:

$$\begin{aligned}
 I &= f(0) d\Omega = \frac{f_{DIS}}{(2\pi)^2 \sqrt{|\Sigma_t|}} d\Omega \\
 &= \frac{f_{DIS}}{(2\pi)^2 \varepsilon_x \varepsilon_y} d\Omega
 \end{aligned} \tag{31}$$

where $d\Omega$ is the solid angle of the collimation system and ε_i are the eigenvalues of the Σ_t -matrix, i.e. the emittances of the transversal degrees of freedom. f_{DIS} is a beam loss factor that quantifies beam losses by deep inelastic (large angle-) scattering.

Hence the transmitted (forward) intensity I is approximately inversely proportional to the product of the emittances and hence depends directly on the strength of proton lateral straggling inside the degrader. The minimal emittances ε_i (and hence the maximal transmission) that can be achieved for a given energy at the degrader exit, depends also on the optical properties on the beam entering the degrader [62, 63], but the emittances of the beam after the collimation system, is mostly determined by the solid angle defined by the apertures of the collimation system. Hence the beam focus as defined by the quadrupoles QMA1, QMA2 and QMA3 (located in front of the degrader), can be used as an additional knobs to control the beam current without having a strong effect on other beam parameters. TRANSPORT is a powerful tool as long as beam losses and emittance increase along the considered beam transport system are negligible. Both of these conditions are not met in cyclotron driven proton therapy facilities, where energy degraders are used to adjust the beam energy, with the side effect to increase the beam emittance beyond the acceptance of the beamline. The use of a degrader implies the necessity to collimate the beam, both transversally (by beam collimation) and in energy spread by an energy selection system (ESS). However this scheme generates a

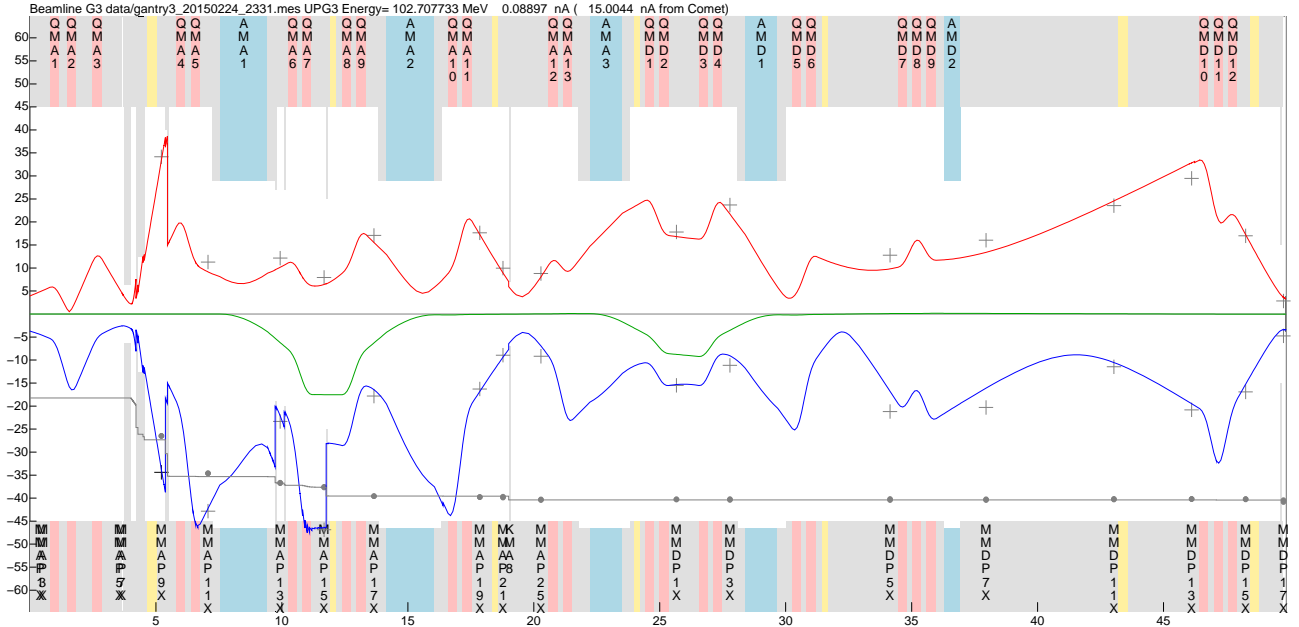


FIG. 11. Beam envelopes ($2\sigma_{rms}$) of the Proscan beamline from proton therapy cyclotron COMET to the entrance of Gantry 3 for an energy of about 100 MeV. The (negative) dispersion is shown in green. The beam width as measured by the proscan beam profile monitors [106, 107] is indicated by crosses. The calculated beam current (i.e. $10 \log(I/\mu A)$) is shown as a solid black line (measurements by gray filled circles). At the end of the beamline, the measured beam current is 90.4 pA agrees well with the MINT result 89 pA.

strong energy dependence of the transmitted beam intensity. Uncompensated, the beam intensity varies between 70 and 250 MeV by roughly three orders of magnitude, for the same cyclotron current. In order to reduce this dynamic intensity range, the beam intensity change is (partially) “compensated” [104]: At low energies, the beam is well-focused onto the degrader in order to provide highest possible transmission. At energies above ≈ 120 MeV, the beam is intentionally defocused on dedicated collimators to reduce the energy dependence of the transmitted intensity.

The intensity compensation at Proscan is done in two stages. The first stage is located upstream of the degrader: QMA3 is used to (de-) focus the beam and to smoothly reduce the transmission of high energies. In order to reduce the dynamic range by two orders of magnitude (from $\approx 10^3$ to ≈ 10), a single stage is not sufficient. A second stage uses the collimator KMA8 for Gantry 3 and, for historical reasons, another collimator KMB0 for Gantry 2. Yet again, the beam is focused to achieve high transmission at low energies and defocused the more the higher the beam energy. Without the second stage compensation, a single beamline tune (set of magnet settings), scaled by momentum, would suffice for all energies. The second compensation stage however requires a slightly different optics setting for each energy and hence a slightly different optical tune for all energies.

Note also that the proton therapy beamlines use some permanent monitors (profile and current) and thin vacuum windows that the beam has to pass [106, 107]. Hence the beam energy after the degrader is not exactly the same as the beam energy entering the nozzle. The effects of these monitors/windows are small but not completely negligible. The beam optics computation done with MINT allows to take these effects into account.

The patient treatment planning system of Proscan always starts with the highest required energy (the deepest layer) and the reduces the energy stepwise for each layer. This is required to avoid hysteresis suppression cycles between

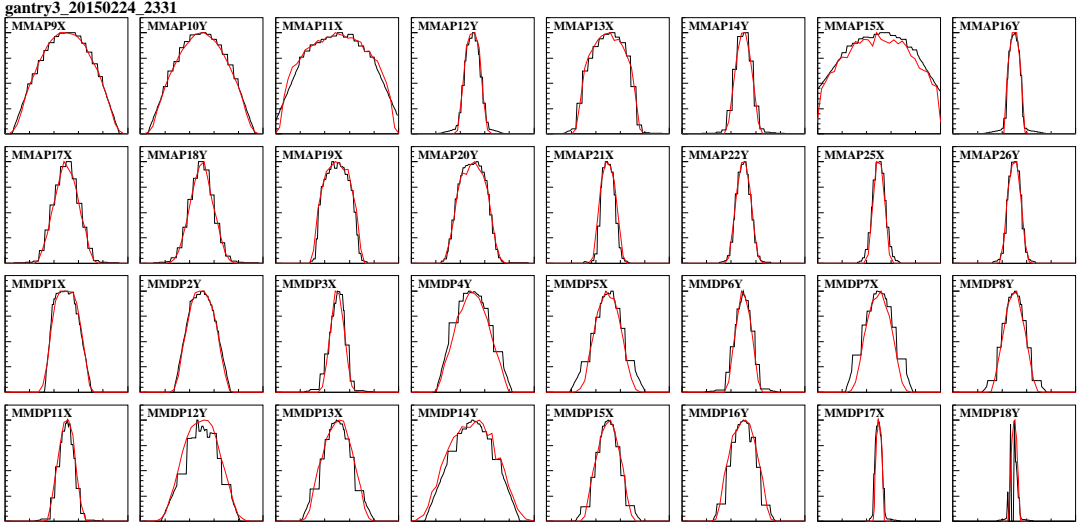


FIG. 12. Simulated (red lines) and measured (black lines) beam profiles corresponding to the measurement shown in Fig. 11. The profiles have been equally scaled and centered for better comparison. (The last measured profile, MMDP18, is distorted due to a bad electrical contact.)

different layers in order to minimize layer switching and hence patient treatment time. The beam tunes should therefore preserve the ramping direction: a reduction of energy should, for all energies, correspond to a decrease of the field-settings of all quadrupoles. Without intensity compensation, the tunes would simply scale the field with the particle momentum and the requirement would be fulfilled automatically, but with active intensity compensation this requirement must be taken into account.

The energy selection system (ESS) consists of a double-bend achromat composed of two dipoles and four quadrupoles. The first dipole generates a non-zero dispersion that is compensated by the second dipole. A moveable collimator (FMA1) is located in the center between the dipoles where the dispersion is maximal, so that the energy spread of the beam can be reduced by adjusting the aperture of the horizontal moveable slit FMA1.

The beamlines to Gantry 1, OPTIS 2 and Gantry 2 are shown in gray, as we shall not discuss their optics here. Gantry 3 shares a beamline with the experimental area of the proton irradiation facility (PIF), which is used only during the night or on weekends, i.e. in times when no patient treatments take place.

MINT enables to model the beam tunes of this type of facility, both qualitatively and quantitatively with reasonable precision. The capability of the code to estimate beam-envelopes and -intensity simultaneously simplifies the design of beamline layout and tunes and allows to predict the transmitted current as well as the locations and the amount of beam loss. The Monte Carlo mode of MINT also enables to predict beam profiles. Significant deviations of the predicted beam profiles from measured profiles helped in the course of the Gantry 3 project to identify errors in the beamline model. Here we show how beam profile and intensity measurements taken during the commissioning shifts for Gantry 3 compare to recalculations lately done with MINT.

Fig. 11 shows a MINT calculation of the Gantry 3 beamline up to the coupling point of Gantry 3. This calculation requires less than 10s with an Monte-Carlo ensemble of 1 Mio. particles on a standard laptop. Simulation results using OPAL of the same beamline have been shown in Ref. [48].

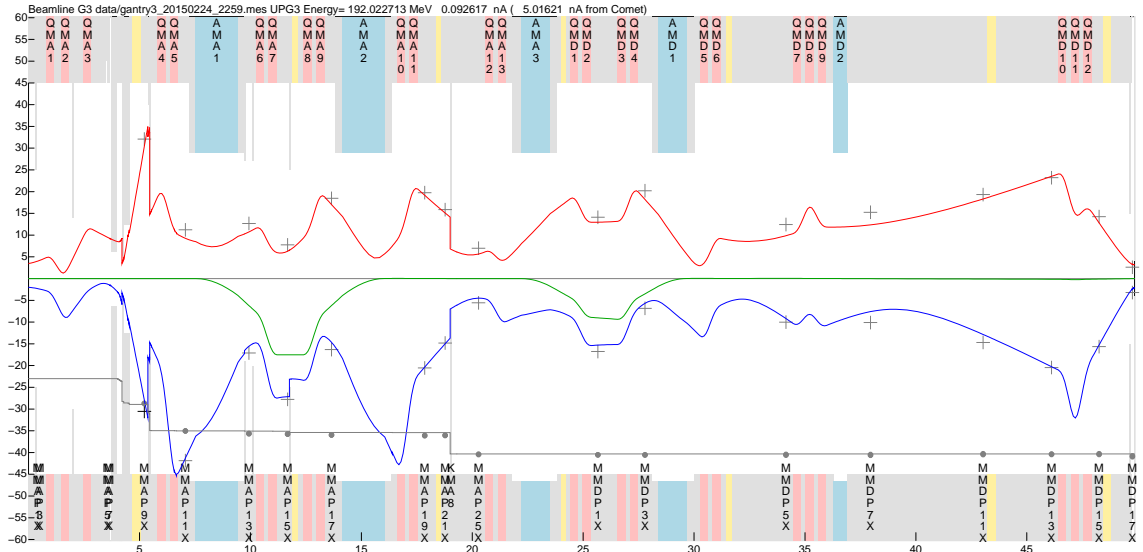


FIG. 13. Same plot as is Fig. 11, but for an energy of ≈ 190 MeV. The intensity is reduced by defocusing the beam vertically with quadrupole QMA3 and after the ESS on collimator KMA8. The Monte Carlo mode starts after the degrader such that the collimator in front of the degrader (after QMA3) has no effect, whereas the collimators behind the degrader (at about $s = 4$ m) and collimator KMA8 (at about $s = 18$ m) reduce both, beam size and current, in agreement with the measurements.

IV. SUMMARY AND OUTLOOK

A description of the methods used in the new ion beam optics program MINT has been given, which allow to extend the applicability of TRANSPORT type calculations to include the passage of matter and beam collimation in a fast and effective way.

The results of various ion beam optics calculations with MINT have been compared with beam profile and intensity measurements of the PSI proton facilities, firstly the high intensity facility HIPA, and secondly of the proton therapy facility Proscan. In all cases MINT provides convenient and fast methods to simulate beam line optics and to compare model and measurement. The accuracy of the ion optics calculation is comparable to TRANSPORT's first order calculations but the range of applicability has been expanded. MINT allows additionally for the simulation of slices of energy degraders or targets and – in the Monte-Carlo-mode – of collimators with simple geometry. It can predict beam losses and realistic beam profiles. The accuracy of these latter calculations is of course limited by the precision of the various multiple scattering approximations. The best agreement with data of the proton therapy facility was obtained using Gottschalk's scattering model [64].

MINT also allows for the calculation of matched beams in ion (storage) rings, cyclotrons, and FFA's for arbitrary couplings and given emittances including space-charge kicks. MINT also allows for the iterative calculation of linear matched beams, even for cyclotron specific couplings, i.e. the so-called “vortex effect”. The correspondings phase space ensembles can be used as starting conditions in other codes like OPAL [89, 90, 92].

MINT does not aim to compete with more “realistic” codes like OPAL or BDSIM. MINT is intended to replace (and extend the capabilities of) the fast and lightweight codes TRANSPORT and TURTLE, specifically as a control

room tool for beamlines like those of PSI’s proton accelerator facilities. MINT has not been (directly) validated by comparison with other codes, but by comparison with profile and current measurements performed at PSI.

V. ACKNOWLEDGEMENTS

We thank Hubert Lutz and Jochem Snuverink for their kind support in installing MINT on the control system computers and Corina Sattler for providing Fig. 1. The other figures have been generated with MINT or with the cernlib (PAW) and XFig, respectively.

MINT has been written in “C++” and compiled with the GNU[©]-C++ compiler on various Linux systems (Scientific Linux, Red Hat 6 & 7 & 8, OpenSuSE 15.X, Ubuntu). MINT uses the GNU[©] scientific library (GSL), and the GNU programs flex and bison. MINT version 0.50, described here, uses GNU libplot for graphical output.

Appendix A: Some Features of MinT

1. The Unit System of MinT

The main purpose of MINT is to provide an alternative to TRANSPORT for the PSI beamlines, both as an online-tool for the machine control rooms but also as a tool to develop tunes for Proscan or layouts for new beamlines.

MINT offers (and to a large degree requires) the definition and the use of units. The predefined unit system is the SI-system, but the user is free to define and use other units, for instance imperial units. MINT automatically scales variables accordingly and checks the consistency of calculations with respect to their physical units: MINT allows to add/subtract or assign only quantities of the same physical dimension. The user not only has the option but is obliged to define the units of all inputs. But he enjoys the freedom to define all parameters in his preferred units and there is no need for the user to convert units “manually”.

MINT comes with a considerable number of pre-defined (SI-) units. Also many “physical constants” are predefined in the form of physical units, for instance the speed of light ‘c’, the elementary charge ‘e’, the mass of the electron ‘Me’ and proton ‘Mp’ and many more. This allows to formulate physical equations in a convenient and readable manner. The MINT syntax expects units written in single quotes in order to distinguish, for instance, ‘m/s’ from a quotient of variables.

Since certain variables, like for instance the pole tip field of a quadrupole magnet, make no sense unless they have the correct unit, MINT allows the user to define variables with a fixed physical meaning, like “MagneticField B” (instead of “Var B”). That is, the type of the physical quantity to be represented by a variable, can be generically taken into account. Hence, strictly speaking, MINT has at least as many basic types as there are different physical quantities and the unit system can be understood as a type checker.

2. The Class/Type System of MinT

The MINT input is based on a simple programming language but provides some features of object-oriented programming. There are predefined “objects”, namely beamline elements like drifts, bends and quads, but additional data fields can be defined and part of their functional behavior can be modified and some basic typing with feature

inheritance has been implemented. MINT allows to create hierarchies of element types by the use of user-defined beamline element classes. If values are specified (assigned) within the type definition, then they are properties of the class and hence, if changed, are changed in all instances of that class. This is due to the fact that variables which are initialized within a type-definition, appear only once in memory and are therefore valid for all instances of the respective type.

```
Type MyQuad(Quad) {
    SHAPE = CIRCULAR;
    Options = OPTLABEL;
    L = 368.0 'mm';
    DS = L/4.0;    // Step size
    R = 50.0 'mm'; // Pole tip radius
    RX = R-5.0 'mm'; // Hor. beam pipe radius
    RY = R-5.0 'mm'; // Vert. beam pipe radius
};

// Since ‘‘Current’’ and ‘‘MagneticField’’ are predefined physical
// quantities, they can be used as if they were basic data types:
Type QMA(MyQuad) {
    Current I,Ilin=101.8 'A',Imax=150.0 'A';
    MagneticField b0 = 34.8 'G' , b1 = 8856.5 'G',
        b2 = -671.4 'G' , b3 = -80.5 'G';
    x:=(abs(I)-Ilin)/(Imax-Ilin);
    B:= sign(I)*(b0 + b1 * abs(I)/Imax +
        (b2 * x^2 + b3 * x^3)*theta_h(abs(I)-Ilin));
};

[...]
Beamline G3 {
[...]
    QMA QMA1 { I= 107.35 'A'; };
};
[...]
```

The length of the quadrupole “QMA” is, as defined here, a property of the class “MyQuad”. If this length is redefined later, this changes the length of all quads of this *class* and hence the length of all quadrupole instances of this type. This allows to fit the parameters not only of individuals but of types; however it requires some care in the definition of the type hierarchy.

The actual definition of quadrupole “QMA1” of type “QMA” requires only to define the coil current to be completed. Since the field value “B” has been (re-) defined, in this example, as a function (indicated by “:=”), it is evaluated on every read access⁶. When the ion optics machinery of MINT reads the quadrupole field in order to compute the transfer matrix, the function “x” is evaluated and hence the field value is effectively a function of the (user-defined) current-variable “I”.

The excitation curve is approximated here by a third order polynomial and from this, the pole tip field is automatically computed, whenever it is used. Since MINT computes the transfer matrix of each element just before the matrix is to be used, one might as well define:

```
Type QMA(Quad) {
    [...]
    MagneticField B0;
```

⁶ In the current version of MINT, this is the only way for the user to define functions.

```

    B:=B0*(PC/('Mp' * 'c' * 'c'));
};
[...]
Beamline G3 {
[...]
    QMA QMA1 { B0 = 7.23 'kG'; };
};

```

where “PC” is the predefined variable of the beam’s actual momentum and “Mp” the projectile (here: proton) mass, so that now the quad field strength is automatically scaled to the momentum and equals “B0” if the momentum (times the speed of light) is equal to $m c^2$ (that is, for $\gamma = \sqrt{2}$ or $\beta = 1/\sqrt{2}$). Since MINT allows for stacked include statements, the user can build up type-libraries for specific kind of problems and easily switch between them by modifying merely the include-statements.

The input script is, like in high-level languages, divided into two parts. The first part provides the definition of element type and a description of the beamline(s). The main part is the “program”, i.e. contains the operations to be performed with the beamline. The main part of a mint-script is translated into a sequence of “byte-codes” which then allows to implement some standard loops (for-do, if-then-else, while-do, repeat-until). The overhead of generating a byte-code and runtime-linking does not significantly increase the execution time, since most of the execution time is usually spend with matrix multiplications.

In order to better compare results with TRANSPORT, MINT provides the possibility to export beamlines to a TRANSPORT type input file. However, due to the different concepts of the two programs, some minor adjustments by hand are usually required before the use with TRANSPORT ⁷.

3. Misalignments in MinT

MINT allows to define a number of misalignments as for instance offsets “Xofs” (horizontal position error) and “Yofs” (vertical position error) and misalignments of the axis *Pitch*, *Yaw* and *Roll*. If these variables are not initialized by the user, they are assumed to be zero. Trivially MINT can, beyond the envelope calculation, calculate, plot and fit the beam centroid as well. These features have been used to determine some (small) quadrupole misalignments within the Proscan facility. Details shall be reported elsewhere.

4. Fitting with MinT

The fitting and optimization functions of MINT are based upon the GNU scientific libraries (GSL) minimization routines. Each beamline-element in MINT is equipped with a *malus*-function which is supposed to quantify the disagreement between the actual state and the desired state of the beamline. Some elements, specifically monitors, have a predefined malus-calculation which computes the (squared) deviation of the calculated and measured beam size, which is activated whenever a non-zero measurement of the beamsize is defined by the user. The malus-functions of other beamline elements must be defined by the user according to their needs.

⁷ For instance, TRANSPORT does not accept layout calculations combined with space charge. The user then has to actively deactivate either of the two before running TRANSPORT.

A typical *malus*-definition within an element-declaration might be ⁸:

```
Malus:=maxError(s11,RX/2.0,0.25 'mm')+maxError(s33,RY/2.0,0.25 'mm');
```

which increases the *malus* in case of a too large beam size, i.e. in cases where $\sigma_x = s11$ and/or $\sigma_y = s33$ are larger than half of the user-defined radius R_x and R_y . The precision is also defined (here 0.25 mm). MINT profile monitors set the respective *malus*-variables to the square deviation, provided that the measured beam size and centroid positions are non-zero.

The *malus* of the beamline is the sum of the *malus* variables of all elements and the minimization of the *malus* is done by the beamline-method *Vary()*:

```
PKSINQ::Vary(@PKSINQ.Malus,@PKSINQ.QHG21.I1,@PKSINQ.QHG21.I2,@PKSINQ.QHG21.I3);
```

where the first argument refers to the *malus*-variable to be minimized and all following parameters are to be varied (the number of parameters to be varied is arbitrary).

MINT is also equipped with an extension of this fitting routine which allows to vary multiply settings “at once”. This is the *MultiVary*-method, in which the *malus* is summed over a set of N calculations before the parameters are varied. This feature can for instance be used, if a parameter can not be fitted based on a single beamline setting. The syntax is:

```
G3::MultiVary(@iTune,17,@G3.Malus,@G3.Protons.s11,@G3.Protons.c12,@G3.Protons.s22);
```

where the first parameter, *iTune*, is an integer variable that indicates the index of the “run”, the second parameter gives the number of “runs” and the remaining parameters are equivalent to *Vary()*, i.e. the *malus*-variable and the parameters to be varied. In the given example, the initial beamsize (of the initial beam named *protons*) is varied using 17 runs. The user then must take care that the respective beamline parameters are properly selected by the iterator “iTune”. Since MINT allows to define *vectors*, *matrices* and (simple) functions, the user can use a construction like the following:

```
Int iTune=0;
Vector qma_fields[4]={ 3.7 'kG', 4.711 'kG', 5.1 'kG', 0.6123 'T' };

Type QMA(Quad) {
  [...]
  B:=qma_fields[iTune];
};

Beamline BL {
  ...
  QMA QMA1;
  ...
};

begin
  BL::MultiVary(@iTune,4,@BL.Malus,@BL.SomeElement.SomeVariable,...);
end.
```

⁸ *maxError* and *minError* are predefined MINT-functions which compute the conditioned squared deviation: The result of *maxError* is zero if the respective value is below the limit.

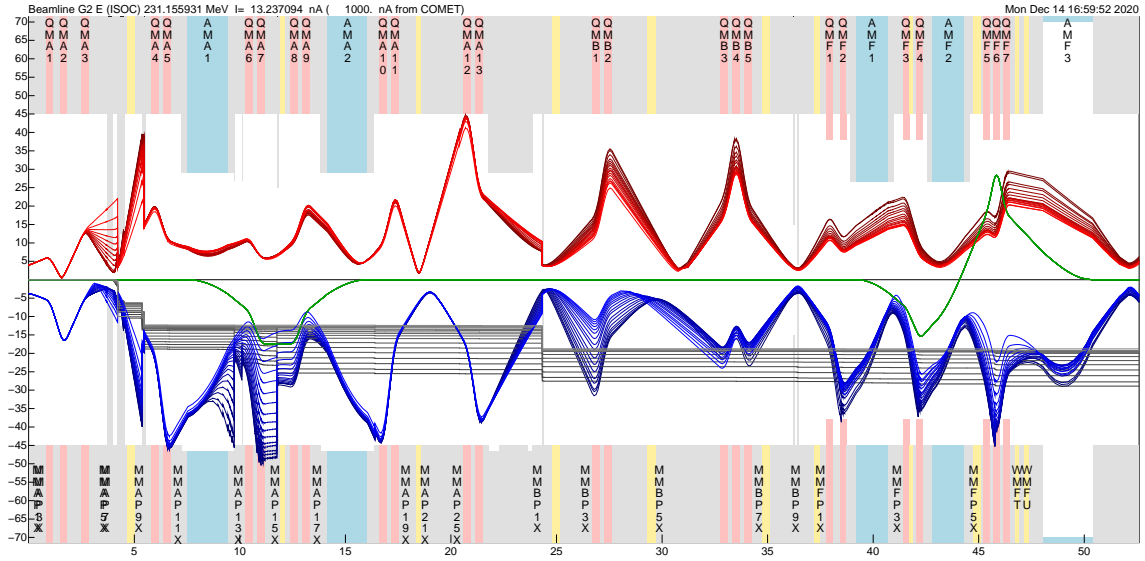


FIG. 14. TRANSPORT style plot of the beam envelopes for a set of tunes for Gantry 2, starting from the cyclotron COMET (left to right) up to the isocenter. The second compensation collimator “KMB0” is located at ≈ 24.5 m downstream of profile monitor “MMBP1X”. Note that the Monte-Carlo mode is here activated *behind* the degrader so that the collimators *before* the degrader are ignored (behind QMA3). This is done on purpose to reduce computation time.

This will cause MINT to sum up the *malus*-variable four times (starting from the initial value) each time, before `@BL.SomeElement.SomeVariable` is varied to minimize the *malus*. This is useful to fit for instance misalignment variables like quadrupole offsets to reproduce *sets* of position measurements for *sets* of quadrupole settings (“beam tunes”).

5. Multiple Plots in MinT

MINT allows to plot a number of runs on a single graph.

Fig. 14 shows for example 17 optimized tunes for the Gantry-2 beamline of Proscan covering the range from 70 MeV to 230 MeV in steps of about 10 MeV thus illustrating the use of the intensity compensation scheme by the use of two collimators located after QMA3 and QMA13, respectively. The energy dependence of the horizontal energy spread and hence the horizontal beam size in the dispersive region between AMA1 and AMA2 is nicely visualized in this plot.

The methods used to do this are:

```
for (k=0;k<17;k+=1) {
  [...]
  G2::Envelope("g2_optics_%d.env"<k);
  G2::PushOptics();
  [...]
};
```

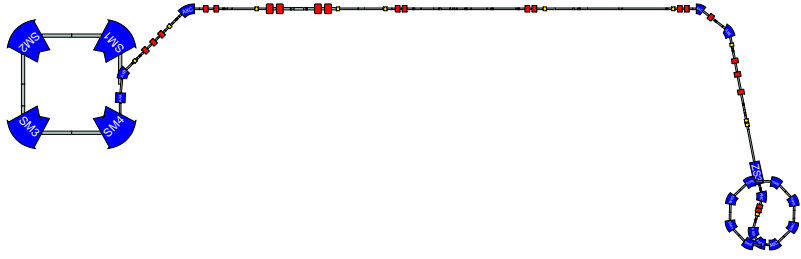


FIG. 15. Layout of the beamline IW2, including the last turn of Injector 2 and the first turn of the Ring cyclotron. (The corresponding beam optics is shown in Fig. 5). This plot was generated from a FIG-file (for the Linux program XFig) produced by MINT, but a direct Postscript output is possible as well.

```
[...]
G2::FlushOptics("X", "", 1200, 600);
G2::FlushOptics("PS", "g2_kmb0_tunes_v1.ps", 12000, 6000);
G2::ClearOptics();
```

6. Layout Calculations and Plots in MinT

MINT allows to compute the floor layout of beamlines and to produce figures illustrating the result. Fig. 15 shows the graphical output produced by MINT-layout routines.

The main purpose of the Layout routines, however, is not to generate beautiful graphics, but to provide numerical layout data to be compared survey data. An example of the output format:

Element	Type	L	S_ref	Z_vertex	Z_traj	X	Y	Z
-	-	'm'	'm'	'm'	'm'	'm'	'm'	'm'
Sec	ISEC	5.494782	0.12875	0.	0.	0.	0.	0.
Valley2b	ZS	1.834156	5.623532	6.540384	6.54061	568.198999	216.619893	1.5
SM2	SM	1.82647	7.457688	8.620229	8.370923	566.119154	216.619893	1.5
Valley3a	ZS	1.834156	9.284158	10.700074	10.201236	566.119154	214.540048	1.5
Valley3b1	Drift	1.351	11.118314	12.292652	11.793814	566.119154	212.94747	1.5
RIZ	ProfZ	0.	12.469314	12.968152	12.469314	566.119154	212.27197	1.5
Valley3b2	Drift	0.48778	12.469314	13.212042	12.713204	566.119154	212.02808	1.5
SM3	SM	1.82647	12.957094	14.618699	13.870329	566.119154	210.621423	1.5
Valley4a	ZS	1.834156	14.783564	16.698543	15.700642	568.198999	210.621423	1.5
Valley4b	ZS	1.834156	16.61772	18.532699	17.534798	570.033155	210.621423	1.5
SM4	SM	1.82647	18.451876	20.612544	19.365111	572.113	210.621423	1.5
MXP1	ProfX20	0.	20.928346	22.425311	20.928346	572.113	212.43419	1.5
AXA	ABend	0.6	20.978346	22.775534	21.278346	572.113	212.784412	1.5
FXE	RDrift	0.	22.431346	23.928756	22.431346	572.221528	213.932516	1.5
AXB	ABend	0.602	22.481346	24.292339	22.782346	572.255744	214.294486	1.5
...								

The output data are aligned with the PSI convention, according to which there are two positions along the beam line. S_{ref} is the measured distance along the actual trajectory and follows the actual path in dipole magnets. Z_{traj}

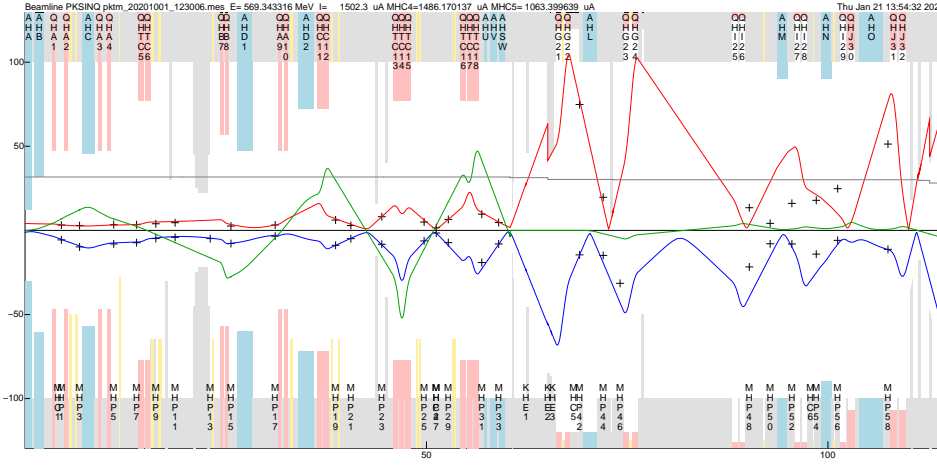


FIG. 16. Computed beam envelope as in Fig. 4, but here without any quadrupole fringe field corrections. The measured beam sizes (symbols) can not be reproduced without a reasonable fringe field correction for large aperture quadrupoles.

is the length of the beam path if described as a polygon connecting the vertices of the bending magnets. It is little more than a convenient measure to compare results with geometric layout data and technical drawings.

Appendix B: Quadrupole Fringe Fields

1. TRANSPORT method (Matsuda/Wollnik)

Note that MINT provides only the linear approximation of the method proposed by Matsuda and Wollnik [83].

Provided the fringe field integrals I_1 , I_2 and I_3 are known according to Rohrer's TRANSPORT convention, the single quadrupole matrix \mathbf{M}_q is embraced by two additional matrices at the quadrupole entrance \mathbf{M}_i and exit \mathbf{M}_f :

$$\mathbf{M}_q \rightarrow \mathbf{M}_f \mathbf{M}_q \mathbf{M}_i. \quad (\text{B1})$$

The horizontal \mathbf{M}_h and vertical \mathbf{M}_v 2×2 -matrices are given by:

$$\mathbf{M}_h = \frac{1}{a} \begin{pmatrix} 1 - x_0 & -x_1 \\ -x_2 & 1 + x_0 \end{pmatrix} \quad (\text{B2})$$

$$\mathbf{M}_v = \frac{1}{b} \begin{pmatrix} 1 + x_0 & x_1 \\ -x_2 & 1 - x_0 \end{pmatrix}$$

where (upper sign for entrance, lower for exit):

$$\begin{aligned} x_0 &= \pm K R^2 I_1 \\ x_1 &= 2 K R^3 I_2 \\ x_2 &= K^2 R^3 I_3 \end{aligned} \quad (\text{B3})$$

where K is the quadrupole strength $K = \frac{B}{R(B\rho)}$, which is positive for horizontally focusing quads. The variables a and b are both equal to 1 in the original calculation. However, 2×2 -matrices are only symplectic, if they have unit determinant. Hence MINT uses:

$$\begin{aligned} a &= \sqrt{1 - x_0^2 - x_1 x_2} \\ b &= \sqrt{1 - x_0^2 + x_1 x_2} \end{aligned} \quad (\text{B4})$$

2. Baartman's approach to quadrupole fringe fields

Baartman's correction [84] is implemented by defining the following variables:

$$\begin{aligned}\Delta\alpha_f &= f_0 k^2 R^2/2 \frac{s^2}{s+\alpha c} & k_f &= k(1 - \frac{\Delta\alpha_f}{\alpha}) \\ \Delta\alpha_d &= f_0 k^2 R^2/2 \frac{S^2}{S+\alpha C} & k_d &= k(1 + \frac{\Delta\alpha_d}{\alpha})\end{aligned}\tag{B5}$$

and from these new values the corrected solutions:

$$\begin{aligned}\alpha &= kL \\ c' &= \cos(\alpha - \Delta\alpha_f) & s' &= \sin(\alpha - \Delta\alpha_f) \\ C' &= \cosh(\alpha + \Delta\alpha_d) & S' &= \sinh(\alpha + \Delta\alpha_d)\end{aligned}\tag{B6}$$

and the corrected (focusing/defocusing) sub-matrices:

$$\begin{aligned}\mathbf{M}_f &= \begin{pmatrix} c' & s'/k_f \\ -k_f' s & c' \end{pmatrix} \\ \mathbf{M}_d &= \begin{pmatrix} C' & S'/k_d \\ k_d S' & C' \end{pmatrix}\end{aligned}\tag{B7}$$

The results of this method for the SINQ-beamline are shown in Fig. 4. If quadrupole fringe fields are ignored, the optics can not be reproduced (See Fig. 16).

-
- [1] Mike Seidel and P.A. Schmelzbach. Upgrade of the PSI Cyclotron Facility to 1.8 MW. In Refuggiato [108], pages 157–162.
 - [2] Mike Seidel, S. Adam, Ch. Baumgarten, J. Bi, R. Dölling, A. Fuchs, M. Humbel, J. Grillenberger, D. Kiselev, A. Mezger, D. Reggiani, M. Schneider, J. Yang, H. Zhang, and T.J. Zhang. Production of a 1.3 Megawatt Proton Beam at PSI. In Noda et al. [109], pages 1309–1313.
 - [3] J. Grillenberger, C. Baumgarten, and M. Seidel. The High Intensity Proton Accelerator Facility. *SciPost Phys. Proc.*, page 2, 2021.
 - [4] E Pedroni *et al.* The 200-MeV proton therapy project at the Paul Scherrer Institute: conceptual design and practical realization. *Med. Phys.*, 22(1):37–53, 1995.
 - [5] F. Atchison *et al.* Production of ultracold neutrons from a cold neutron beam on a $^2\text{H}_2$ target. *Phys. Rev. C*, 71:054601, 2005.
 - [6] A. Anghel *et al.* The psi ultra-cold neutron source. *Nuclear Instruments and Methods in Physics Research Section A: Accelerators, Spectrometers, Detectors and Associated Equipment*, 611(2):272–275, 2009. Particle Physics with Slow Neutrons.
 - [7] B. Lauss and the PSI UCN Project Team. Commissioning of the new high-intensity ultracold neutron source at the paul scherrer institut. *Journal of Physics: Conference Series*, 312(052005), 2011.
 - [8] Bernhard Lauss. Startup of the high-intensity ultracold neutron source at the paul scherrer institut. In P. Bühler, O. Hartmann, K. Suzuki, E. Widmann, and J. Zmeskal, editors, *Proceedings of EXA 2011*, pages 297–301. Springer, Dordrecht, Netherlands, 2012.
 - [9] Bernhard Lauss. Ultracold neutron production at the second spallation target of the paul scherrer institut. *Physics Procedia*, 51:98–101, 2014.

- [10] R. M. Bergmann, U. Filges, D. Kiselev, T. Reiss, V. Talanov, and M. Wohlmuther. Upgrades to the sinq cold neutron source. *J. of Phys. Conf. Ser.*, 746:012035, 2015.
- [11] G. Bison, B. Blau, M. Daum, L. Göttl, R. Henneck, K. Kirch, D. Lauss, B. and Ries, P. Schmidt-Wellenburg, and G. Zsigmond. Neutron optics of the psi ultracold-neutron source: characterization and simulation. *The European Physical Journal A*, 56(2):33, Feb 2020.
- [12] D. Kiselev, P. Baumann, B. Blau, K. Geissmann, D. Laube, T. Reiss, R. Sobbia, A. Strinning, V. Talanov, and M. Wohlmuther. The meson target stations and the high power spallation neutron source SINQ at PSI. *J. Radioanal. Nucl. Chem.*, 305:769–775, 2015.
- [13] F. Berg, L. Desorgher, A. Fuchs, W. Hajdas, Z. Hodge, P.-R. Kettle, A. Knecht, R. Lüscher, A. Papa, G. Rutar, and M. Wohlmuther. Target studies for surface muon production. *Phys. Rev. Accel. Beams*, 19:024701, 2016.
- [14] D. Kiselev, P. A. Duperrex, S. Jollet, S. Joray, D. Laube, D. Reggiani, R. Sobbia, and V. Talanov. The Meson Production Targets in the high energy beamline of HIPA at PSI. *SciPost Phys. Proc.*, page 3, 2021.
- [15] G. S. Bauer, W. E. Fischer, U. Rohrer, and U. Schryber. Commissioning of the 1 mw spallation neutron source SINQ. In *Proceedings of the 1997 Particle Accelerator Conference (PAC 97)*, pages 3785–3787, Piscataway, NJ, May 12-16 1997. IEEE.
- [16] Günter S. Bauer. Operation and development of the new spallation neutron source sinq at the paul scherrer institut. *Nuclear Instruments and Methods in Physics Research Section B: Beam Interactions with Materials and Atoms*, 139(1):65–71, 1998.
- [17] Y. Dai and G. S. Bauer. Status of the first SINQ irradiation experiment, STIP-I. *J. Nucl. Mat.*, 296:43–53, 2001.
- [18] W. Wagner, J. Mesot, P. Allenspach, G. Kuehne, and H. M. Ronnow. The swiss spallation neutron source SINQ developments and upgrades for optimized user service. *Physica B*, 385-386:968–971, 2006.
- [19] Werner Wagner, Yong Dai, Heike Glasbrenner, Mirco Grosse, and Eberhard Lehmann. Status of sinq, the only mw spallation neutron source—highlighting target development and industrial applications. *Nucl. Instr. Meth. A*, 562(2):541–547, 2006.
- [20] B. Blau *et al.* The swiss spallation neutron source sinq at paul scherrer institut. *Neutron News*, 20(3):5–8, 2009.
- [21] H. Blosser *et al.* Proposal for a manufacturing prototype superconducting cyclotron for advanced cancer therapy. *MSUCL-874*, 1993.
- [22] M. Schillo, A. Geisler, A. Hobl, H.U. Klein, M. Meyer-Reumers, H. Blosser, J.-W. Kim, F. Marti, J. Vincent, S. Brandenburg, and J.P.M. Beijers. Compact Superconducting 250 MeV Proton Cyclotron for the PSI PROSCAN Therapy Project. In F. Marti, editor, *Proceedings of the 16th International Conference on Cyclotrons and their Applications*, volume 16, pages 37–39. American Institute of Physics (2001), may 13-17 2001.
- [23] A. Geisler, C. Baumgarten, A. Hobl, U. Klein, D. Krischel, M. Schillo, and J. Timmer. Status Report of the ACCEL 250 MeV Medical Cyclotron. In Akira Goto, editor, *Proceedings of the 17th International Conference on Cyclotrons and their Applications*, page 541. Part. Accel. Soc. Japan (2004), oct 2004.
- [24] Hans-Udo Klein, Christian Baumgarten, Andreas Geisler, Jürgen Heese, Achim Hobl, Detlef Krischel, Michael Schillo, Stefan Schmidt, and Jan Timmer. New superconducting cyclotron driven scanning proton therapy systems. *Nucl. Instrum. Meth. B*, 241(1):5013108, 2005.
- [25] A.E. Geisler, J. Hottenbacher, H.-U. Klein, D. Krischel, H. Röcken, M. Schillo, T. Stephani, J.H. Timmer, and C. Baumgarten. Commissioning of the ACCEL 250 MeV Proton Cyclotron. In Refuggiato [108].
- [26] D. Krischel *at al.* Design aspects and operation experience with a novel superconducting cyclotron for cancer treatment. *IEEE Trans. Appl. Supercond.*, 17(2):2307–2310, 2007.
- [27] C. Baumgarten, A. Geisler, U. Klein, D. Krischel, H. Röcken, M. Schillo, T. Stephani, and J.H. Timmer. Isochronism of the ACCEL 250MeV medical proton cyclotron. *Nucl. Instrum. Meth. A*, 570(1):10–14, 2007.

- [28] Marco Schippers, Jürgen Duppich, Gurdrun Goitein, Eugen Hug, Martin Jermann, Anton Mezger, and Eros Pedroni. First year of operation of PSI's new sc cyclotron and beamlines for proton therapy. In Refuggiato [108].
- [29] J.M. Schippers, R. Dölling, J. Duppich, G. Goitein, M. Jermann, A. Mezger, E. Pedroni, H.W. Reist, and V. Vrankovic. The sc cyclotron and beam lines of PSI's new protontherapy facility proscan. *Nucl. Instrum. Meth. B*, 261(1):773–776, 2007.
- [30] Urs Rohrer. Graphic TRANSPORT Framework. *Online Manual* (<http://aea.web.psi.ch/Urs-Rohrer/MyWeb/trans.htm>), 2007.
- [31] K.L. Brown, D.C. Carey, Ch. Iselin, and F. Rothacker. Transport, a computer program for designing charged particle beam transport systems. Technical Report 73-16, CERN, Geneva, Switzerland, Nov 1973.
- [32] Ch. Iselin K.L. Brown, D.C. Carey and F. Rothacker. Transport, a computer program for designing charged particle beam transport systems. Technical Report 80-4, CERN, Geneva, Switzerland, Mar 1980.
- [33] K.L. Brown and Ch. Iselin. Decay turtle, a computer program for simulating charged particle beam transport systems, including decay calculations. Technical Report 74-02, CERN, Geneva, Switzerland, Feb 1974.
- [34] D.C. Carey, K.L. Brown, and Ch. Iselin. Decay turtle, a computer program for simulating charged particle beam transport systems, including decay calculations. Technical Report 246 UC-28, SLAC, Stanford, California, Mar 1982.
- [35] Andreas Adelman, Ch. Kraus, Y. Ineichen, S. Russell, Y. Bi, and J.J. Yang. The object oriented parallel accelerator library (opal), design, implementation and application. In Joe Chew, editor, *Proceedings of the 10th International Conference on Computational accelerator physics (ICAP'09)*, page 258, Berkeley, USA, August 31-September 4 2009. LBL.
- [36] Andreas Adelman, S. Binder, Ch. Kraus, Y. Ineichen, T. Schietinger, S. Russell, and J.J. Yang. The object oriented parallel accelerator library (opal). In Martin Comyn, Shane Koscielniak, Volker R. W. Schaa, and Paul W. Schmor, editors, *Proceedings of the 23rd Particle accelerators Conference (PAC'09)*, page 5076, Geneva, Switzerland, 2009. JACoW.
- [37] J. J. Yang, A. Adelman, M. Humbel, M. Seidel, and T. J. Zhang. Beam dynamics in high intensity cyclotrons including neighboring bunch effects: Model, implementation, and application. *Phys. Rev. ST Accel. Beams*, 13:064201, Jun 2010.
- [38] Y. J. Bi, A. Adelman, R. Dölling, M. Humbel, W. Joho, M. Seidel, and T. J. Zhang. Towards quantitative simulations of high power proton cyclotrons. *Phys. Rev. ST Accel. Beams*, 14:054402, May 2011.
- [39] Andreas Adelman, Pedro Calvo, Matthias Frey, Achim Gsell, Uldis Locans, Christof Metzger-Kraus, Nicole Neveu, Chris Rogers, Steve Russell, Suzanne Sheehy, Jochem Snuverink, and Daniel Winklehner. Opal a versatile tool for charged particle accelerator simulations, 2019.
- [40] S. Agostinelli *et al.* Geant4—a simulation toolkit. *Nuclear Instruments and Methods in Physics Research Section A: Accelerators, Spectrometers, Detectors and Associated Equipment*, 506(3):250–303, 2003.
- [41] J. Allison *et al.* Geant4 developments and applications. *IEEE Transactions on Nuclear Science*, 53(1):270–278, Feb 2006.
- [42] J. Allison *et al.* Recent developments in geant4. *Nuclear Instruments and Methods in Physics Research Section A: Accelerators, Spectrometers, Detectors and Associated Equipment*, 835:186–225, 2016.
- [43] L.J. Nevay, S.T. Boogert, J. Snuverink, A. Abramov, L.C. Deacon, H. Garcia-Morales, H. Lefebvre, S.M. Gibson, R. Kwee-Hinzmann, W. Shields, and S.D. Walker. Bdsim: An accelerator tracking code with particle–matter interactions. *Computer Physics Communications*, 252:107200, 2020.
- [44] C. Baumgarten. *MinT User Manual*. Paul Scherrer Institute, Villigen, Switzerland, 2020.
- [45] A. Koschik, C. Bula, J. Duppich, A. Gerbershagen, M. Grossmann, J.M. Schippers, and J. Welte. Gantry 3: Further development of the PSI PROSCAN proton therapy facility. In Stuart Henderson, Todd Satogata, and Volker R. W. Schaa, editors, *Proceedings of the 6th International Conference Particle accelerator (IPAC 2015)*, Geneva, Switzerland, May 3-8 2015. JACoW.
- [46] A. Koschik, C. Baumgarten, C. Bula, J. Duppich, A. Gerbershagen, M. Grossmann, V. Rizzoglio, and J. Welte. PSI

- gantry 3: Integration of a new gantry into an existing proton therapy facility. In Kyung Sook Kim, In Soo Ko, Kyung Ryul Kim, and Volker R. W. Schaa, editors, *Proceedings of the 7th International Particle accelerator Conference (IPAC 2016)*, Geneva, Switzerland, May 8-13 2016. JACoW.
- [47] A. Koschik, J. Duppich, M. Eichin, P. Fernandez, A. Gerbershagen, A. Lomax, D. Meer, S. Safai, J. M. Schippers, and D. C. Weber. Status of commissioning of GANTRY 3 at the PSI proscan facility. In Volker R. W. Schaa, Gianluigi Arduini, Mats Lindroos, and Juliana Pranke, editors, *Part 2, Proceedings of the 8th International Particle accelerator Conference (IPAC 2017)*, volume 874, Geneva, Switzerland, May 14-19 2017. JACoW.
- [48] V. Rizzoglio, A. Adelmann, C. Baumgarten, M. Frey, A. Gerbershagen, D. Meer, and J. M. Schippers. Evolution of a beam dynamics model for the transport line in a proton therapy facility. *Phys. Rev. Accel. Beams*, 20(12):124702, 2017.
- [49] Christian Baumgarten, Valeria Rizzoglio, and Alexander Gerbershagen. The Proscan Gantry 3 Proton Therapy Beamline. *The XXXIX. European Cyclotron Progress Meeting (ECPM), UCL, Louvaine-la-Neuve, Belgium*, Sep. 2015.
- [50] Christian Baumgarten. A symplectic method to generate multivariate normal distributions. *arXiv:1205.3601*, 2012.
- [51] Wioletta Wieszczycka and Waldemar H. Scharf. *Proton Radiotherapy Accelerators*. World Scientific, 2001.
- [52] Alexander W. Chao and Weiren Chou, editors. *Reviews of Accelerator Science and Technology Vol. 2 – Medical Applications of Accelerators*. World Scientific, 2009.
- [53] Wayne D. Newhauser and Rui Zhang. The physics of proton therapy. *Phys. Med. Biol.*, 60:R155–R209, 2015.
- [54] Marco Durante and Harald Paganetti. Nuclear physics in particle therapy: a review. *Rep. Progr. Phys.*, 79:096702, 2016.
- [55] Harald Paganetti (Edt.), editor. *Proton Therapy Physics*. CRC Press (Taylor & Francis), 2012.
- [56] D.E. Groom and S.R. Klein. Passage of particles through matter. *Eur. Phys. J. C*, 15:163–173, 2000.
- [57] A.A. Bednyakov, Yu. V. Bulgakov, V.S. Nikolaev, V.P. Sobakin, and B.M. Popov. Stopping-power distribution for fast helium and nitrogen ions passing through metal films. *Sov. Phys.-JETP*, 41(6):1034–1037, 1976.
- [58] W.R. Leo. *Techniques for Nuclear and Particle Physics*. Springer, Berlin Heidelberg, 1994.
- [59] R.K. Tripathi, Francis A. Cucinotta, and John W. Wilson. Accurate universal parameterization of absorption cross sections. *Nuclear Instruments and Methods in Physics Research Section B: Beam Interactions with Materials and Atoms*, 117(4):347–349, 1996.
- [60] R.K. Tripathi, John W. Wilson, and Francis A. Cucinotta. Accurate universal parameterization of absorption cross sections ii — neutron absorption cross sections. *Nuclear Instruments and Methods in Physics Research Section B: Beam Interactions with Materials and Atoms*, 129(1):11–15, 1997.
- [61] R.K. Tripathi, F.A. Cucinotta, and J.W. Wilson. Accurate universal parameterization of absorption cross sections iii – light systems. *Nuclear Instruments and Methods in Physics Research Section B: Beam Interactions with Materials and Atoms*, 155(4):349–356, 1999.
- [62] Francis J.M. Farley. Degradation and ionization cooling. *Nucl. Phys. B (Proc. Suppl.)*, 149:289–294, 2005.
- [63] Francis J.M. Farley. Optimum strategy for energy degraders and ionization cooling. *Nucl. Instr. Meth. A*, 540:235–244, 2005.
- [64] B. Gottschalk. On the scattering power of radiotherapy protons. *Med. Phys.*, 37(1):352–367, 2009.
- [65] C. Baumgarten, A. Barchetti, H. Einkenkel, D. Goetz, and P.A. Schmelzbach. A compact electron cyclotron resonance proton source for the Paul Scherrer Institute’s proton accelerator facility. *Rev. Sci. Instrum.*, 82:053304, 2011.
- [66] S. Adam, B. Berkes, D. Collins, P. Lanz, M. Olivo, and U. Schryber. A proposed new injector for the S.I.N. ring cyclotron. In Joho [110], pages 123–126.
- [67] M. Olivo, W. Joho, and U. Schryber. The design of an 860 keV pre-accelerator for the new SIN high current injector cyclotron. In *Proceedings, 1979 Particle Accelerator Conference: Accelerator Engineering and Technology*, volume 26, pages 3980–3982, New York, March 12-14 1979. IEEE.
- [68] U. Schryber, S. Adam, B. Berkes, H. Frei, W. Joho, P. Lanz, C. Markovits, M. Olivo, L. Rezzonico, and N. Schmid.

- Status report on the new injector at SIN. In Gendreau [111], pages 43–53.
- [69] W. Joho, S. Adam, B. Berkes, T. Blumer, M. Humbel, P. Lanz, C. Markovits, A. Mezger, M. Olivo, L. Rezzonico, U. Schryber, and P. Sigg. Commissioning of the new high intensity 72 MeV injector II for the SIN ring cyclotron. In A. Strathdee, editor, *Proceedings of the 1985 Particle Accelerator Conference (PAC1985)*, volume 32, pages 2666–2668, Piscataway, NJ, March 13-16 1985. IEEE.
- [70] Ch. Markovits. The 870 keV high intensity proton beam transfer line for the injector II of SIN. In E. R. Lindstrom and L. S. Taylor, editors, *Proceedings of the 1987 IEEE Particle Accelerator Conference (PAC1987)*, volume 3, pages 1954–1956, Piscataway, NJ, March 16-19 1987. IEEE.
- [71] J. Stetson, S. Adam, M. Humbel, W. Joho, and Th. Stammbach. The commissioning of PSI injector 2 for high intensity, high quality beams. In G. Dutto and M.K. Craddock, editors, *Proceedings of the 13th International Conference on Cyclotrons and their Applications*, pages 36–39. World Scientific, jul 1992.
- [72] H. A. Willax. Proposal for a 500 MeV Isochronous Cyclotron with Ring Magnet. In F.T. Howard and N. Vogt-Nilsen, editors, *CERN Report 63-19*, pages 386–397. CERN, April 1963.
- [73] J. P. Blaser, H. A. Willax, and H.-J. Gerber. The S.I.N. ring cyclotron project status report. In Samuel Devons, editor, *High-Energy Physics and Nuclear Structure*, pages 556–565, Boston, MA, 1970. Springer US.
- [74] H. A. Willax. Status report of SIN ring cyclotron. In J.J. Burgerjon and A. Strathdee, editors, *AIP Conference Proceedings No. 9 (1972)*, pages 114–125. American Institute of Physics (1971), Jul 1972.
- [75] H. A. Willax. Present status of the 590 MeV ring cyclotron of S.I.N. In E. J. Lofgren, editor, *Proceedings, 1973 Particle Accelerator Conference, Accelerator Engineering and Technology*, volume 20, pages 202–206, New York, March 5-7 1973. IEEE.
- [76] W. Joho. The S.I.N. ring cyclotron after one year of operation. In Joho [110], pages 1397–1401.
- [77] S. Adam. The isochronism in the S.I.N. 590 mev ring cyclotron. In Joho [110], pages 283–286.
- [78] W. Joho and S. Adam. Setting up the s.i.n. 590 mev ring cyclotron for single turn extraction. In J.W. Hicks, editor, *Proceedings of the 8th International Conference on Cyclotron and their Applications*, volume 24, pages 2358–2361. IEEE, August 1978.
- [79] D. Reggiani, D. Kiselev, T. Reiss, R. Sobbia, V. Talanov, and M. Wohlmuther. Beam transport optimization studies of the PSI MW-class proton channel. In Christine Petit-Jean-Genaz, Gianluigi Arduini, Peter Michel, and Volker R. W. Schaa, editors, *Proceedings of the 5th International Particle accelerator Conference (IPAC 2014)*, JACoW conferences, pages 1189–1191, Geneva, Switzerland, June 15-20 2014. CERN.
- [80] Y. Lee, D. Reggiani, M. Gandel, D.C. Kiselev, P. Baumann, and M. Seidel. New design of a collimator system at the PSI proton accelerator. In Andreas Adelmann, Jan Chrin, Michaela Marx, Volker R. W. Schaa, and Mike Seidel, editors, *Proceedings of the 46th ICFA Advanced Beam Dynamics Workshop on High-Intensity and High-Brightness Hadron Beams (HB2010)*, pages 567–571, Villigen, Switzerland, September 27-October 1 2010. PSI.
- [81] Y. Lee, M. Gandel, D. Reggiani, M. Seidel, and S. Teichmann. Simulation based optimization of a collimator system at the PSI proton accelerator facility. In Noda et al. [109], pages 4260–4262.
- [82] D. Reggiani, D. Kiselev, M. Seidel, V. Talanov, and M. Wohlmuther. Combined MCNP/TURTLE simulation of the SINQ beamline at PSI-HIPA. In Mark Boland, Hitoshi Tanaka, David Button, and Rohan Dowd, editors, *Proceedings of the 10th International Particle accelerator Conference (IPAC 2019)*, volume 1350, pages 2410–2413, Geneva, Switzerland, May 19-24 2019. JACoW.
- [83] H. Matsuda and H. Wollnik. Third order transfer matrices for the fringing field of magnetic and electrostatic quadrupole lenses. *Nucl. Instrum. Meth*, 103:117–124, 1972.
- [84] Rick Baartman. Short quadrupole parameterization. In C. Petit-Jean-Genaz, editor, *Proceedings of PAC '07*, pages 3229–3231. IEEE, June 25-29 2007.

- [85] Y. J. Bi, A. Adelman, R. Dölling, M. Humbel, W. Joho, M. Seidel, and T. J. Zhang. Towards quantitative simulations of high power proton cyclotrons. *Phys. Rev. ST Accel. Beams*, 14:054402, May 2011.
- [86] U. Schryber, S. Adam, T. Blumer, J. Cherix, H.R. Fitze, H. Frei, D. George, G. Heidenreich, M. Humbel, I. IIROUSEK, W. Joho, M. Marki, C. Morkovits, A. Mezger, M. Olivo, L. Rezzonico, U. Rohrer, P. Sigg, and T. Stammach. High power operation of the PSI accelerators. In Comell [112], page 858.
- [87] S. Adam. Space charge effect in cyclotrons - from simulations to insights. In Comell [112], page 858.
- [88] J.J. Yang, A. Adelman, M. Humbel, M. Seidel, and T.J. Zhang. Numerical study of beam dynamics in high intensity cyclotrons including neighboring bunch effects. In Stuart Henderson, editor, *Proceedings of the 42nd ICFA Advanced Beam Dynamics Workshop on High-Intensity, High-Brightness Hadron Beams (HB 2008)*, Oak Ridge, USA, August 25-29 2008. Oak Ridge Nat. Lab.
- [89] C. Baumgarten. Transverse-longitudinal coupling by space charge in cyclotrons. *Phys. Rev. ST Accel. Beams*, 14:114201, Nov 2011.
- [90] C. Baumgarten. Transverse-longitudinal coupling by space charge in cyclotrons. In Jana Thomson and Volker Schaa, editors, *Proceedings of the 20th International Conference on Cyclotrons and their Applications*, pages 316–319. JaCoW, jul 2013.
- [91] A. Kolano, A. Adelman, R. Barlow, and C. Baumgarten. Intensity limits of the PSI injector II cyclotron. *Nucl. Instrum. Meth. in Phys. Res. A*, 885:54–59, 2018.
- [92] C. Baumgarten. Factors influencing the vortex effect in high-intensity cyclotrons. In Lowry Conradie, John Garrett De Villiers, and Volker R. W. Schaa, editors, *Proceedings, 22nd International Conference on Cyclotrons and their Applications, Cyclotrons 2019: Cape Town, South Africa, 23-27 September 2019*, pages 270–274, JACoW, 1 2019. Geneva, Switzerland.
- [93] C. Baumgarten. Use of real dirac matrices in two-dimensional coupled linear optics. *Phys. Rev. ST Accel. Beams*, 14:114002, Nov 2011.
- [94] C. Baumgarten. Geometrical method of decoupling. *Phys. Rev. ST Accel. Beams*, 15:124001, Dec 2012.
- [95] Christian Baumgarten. A Jacobi Algorithm in Phase Space: Diagonalizing (skew-) Hamiltonian and Symplectic Matrices with Dirac-Majorana Matrices. *arXiv:2008.13409*, 2020.
- [96] Ch. Markovits. Design of a high intensity 860 keV proton beam transport line for the new SIN injector. In Gendreau [111], pages 525–527.
- [97] M. Olivo. Initial operation of the SIN 860 keV cockcroft-walton pre-injector. In N. Angert, editor, *Proceedings of the Linear Accelerator Conference (Linac'84)*, pages 380–382, Darmstadt, 5 1984. GSI.
- [98] M. Olivo. Operational Experience with the SIN 870 keV Cockcroft-Walton Pre-Injector. In M. Sekiguchi, Y. Yano, and K. Hatanaka, editors, *Proceedings of the 11th International Conference on Cyclotron and their Applications*, pages 519–522. Ionics Publ., Tokyo (1987), September 1986.
- [99] J. Grillenberger, M. Humbel, J. Y. Raguin, and P. A. Schmelzbach. Commissioning of the new buncher system in the 870 keV injection beamline. In Refuggiato [108], pages 464–466.
- [100] Eros Pedroni, Ralph Bearpark, Terence Böhringer, Adolf Coray, Jürgen Duppich, Sven Forss, David George, Martin Grossmann, Gudrun Goitein, Christian Hilbes, Martin Jermann, Shixiong Lin, Antony Lomax, Marco Negrazus, Marco Schippers, and Goran Kotrle. The PSI gantry 2: a second generation proton scanning gantry. *Z. f. Med. Phys.*, 14(1):25–34, 2004.
- [101] Sairos Safai, Christian Bula, David Meer, and Eros Pedroni. Improving the precision and performance of proton pencil beam scanning. *Translational Cancer Research*, 1(3), 2012.
- [102] M.J. van Goethem, R. van der Meer, H.W. Reist, and J.M. Schippers. Geant4 simulations of proton beam transport through a carbon or beryllium degrader and following a beam line. *Phys. Med. Biol.*, 54:5831–5846, 2009.

- [103] E. Pedroni and H. Enge. Beam optics design of compact gantry for proton therapy. *Med. & Biol. Eng. & Comput.*, 33:271–277, 1995.
- [104] D. Meer E. Pedroni, C. Bula, S. Safai, and S. Zenklusen. Pencil beam characteristics of the next-generation proton scanning gantry of PSI: design issues and initial results. *Eur. Phys. J. Plus*, 126(66), 2011.
- [105] W. Hajdas, F. Burri, C. Eggel, R. Harboe-Sorensen, and R. de Marino. Radiation effects testing facilities in PSI during implementation of the proscan project. In *IEEE Radiation Effects Data Workshop*, pages 160–164, July 2002.
- [106] R. Dölling. Diagnostics of the proscan proton-therapy beam lines. In Andreas Peters and Volker R. W. Schaa, editors, *Beam diagnostics and instrumentation for particle accelerators. Proceedings, 6th European Workshop, DIPAC 2003*, pages 152–154, Darmstadt, Germany, May 5-7 2003. GSI.
- [107] R. Dölling. Profile, current, and halo monitors of the proscan beam lines. In Thomas Shea and R. Coles Sibley III, editors, *AIP Conference Proceedings 732*, pages 244–252. AIP, May 3-6 2004.
- [108] D. Refuggiato, editor. *18th International Conference on Cyclotrons and their Applications*. INFN - LNS Catania, Italy (2008), October 2007.
- [109] Akira Noda, Christine Petit-Jean-Genaz, Volker R. W. Schaa, Toshiyuki Shirai, and Akihiro Shirakawa, editors. Geneva, Switzerland, May 23-28 2010. JACoW.
- [110] W. Joho, editor. *7th International Conference on Cyclotron and their Applications*. Birkhäuser, Basel CH, August 1975.
- [111] G. Gendreau, editor. *9th International Conference on Cyclotron and their Applications*. Les Editions de Physique, BP 112, 91402 Orsay (France), September 1981.
- [112] J. Comell, editor. *14th International Conference on Cyclotrons and their Applications*. World Scientific, oct 1995.